



## Experimental and theoretical investigations on the use of *Corchorus olitorius* stem extract as a safe corrosion inhibitor for carbon steel in hydrochloric acid

Marzough A Albalawi<sup>1</sup>, H.S.Gadow<sup>2\*</sup>

<sup>1</sup> University of Tabuk, Alwajh college, Department of Chemistry, Saudi Arabia.

<sup>2\*</sup> Higher Institute for Engineering and Technology, Department of Chemistry, New Damietta, Egypt.



CrossMark

### Abstract

The adsorption activity and inhibitory effect of *Corchorus olitorius* stem extract (ECS) were investigated as a safe inhibitor for the dissolution of carbon steel in a 1 M hydrochloric acid solution. In this study, different electrochemical techniques, such as electrical frequency modulation, potentiodynamic polarisation, electrochemical impedance spectroscopy, a chemical method (gravimetric method), and theoretical investigation, were all applied. Along with these approaches, we used a variety of other strategies to look at the surface morphology of carbon steels (AFM, XPS, and FTIR). This extract is a mixed-type inhibitor, according to the results of the polarisation technique measurements. Parameters related to thermodynamics were calculated and discussed. The adsorption of *Corchorus olitorius* obeys the Langmuir and Temkin adsorption isotherms stems extract on the alloy. Using a gravimetric technique, the extract provides a fantastic inhibitory efficiency of 95.53% at 300 ppm from *Corchorus olitorius* stems. The computed I.E.% from experiments and the theoretical studies were found to be related. The location of sterols and fatty acids has long been determined using the molecular electrostatic potential (MESP).

Keywords: corrosion; carbon steel; electrochemistry; theoretical study.

### 1. Introduction

Due to its accessibility, low cost, and favourable physio-chemical characteristics [1], various applications typically use carbon steel, including those related to construction, and equipment for processing and manufacturing [2, 3]. The most significant issue with using carbon steel in industrial applications is corrosion. When exposed to a hostile environment, metallic materials deteriorate [4]. The hydrochloric solution is commonly used for industrial cleaning, acid pickling, and descaling [5,6]. However, when corrosion happens due to the use of acid, it can lead to numerous financial issues. Corrosion costs the world's economies approximately US \$2.5 trillion annually [7]. Corrosion expenses are divided into direct and indirect costs [8]. To solve this issue, several strategies have been employed. Using organic compounds—especially heterocyclic compounds—is a cost-efficient and successful way to reduce

corrosion. Coating, painting, alloying, dealloying, and galvanising are examples of current techniques that can help cut the cost of corrosion by 15% to 35% [7]. Due to its effectiveness and widespread applicability in many industries, corrosion inhibitors are one of the most common approaches [9,10]. When modest doses of corrosion inhibitors are introduced to the acid media, metal dissolution is reduced [11]. Corrosion is effectively inhibited by several synthesized chemical inhibitors [12, 13]. Synthetic compounds having electronegative elements like nitrogen, oxygen, phosphorus, and sulphur, plan conjugate arrangements with different aromatic rings, and unsaturated bonds make up the majority of anticorrosion agents, too, organic corrosion inhibitors can delay active dissolving sites in addition to forming thick protective coating on metal surfaces. These adhere to the metal surface and stop steel from corroding [14]. Little dosage, high corrosion prevention effect, and ease of use are all benefits of corrosion inhibitors. Scientists

\*Corresponding author e-mail: [hsgado73@gmail.com](mailto:hsgado73@gmail.com); (Hend Gadow).

Received date 15 November 2023; revised date 30 January 2024; accepted date 18 February 2024

DOI: 10.21608/ejchem.2024.249091.8882

©2019 National Information and Documentation Center (NIDOC)

working on corrosion protection have therefore given it a lot of attention. While having many benefits, many corrosion inhibitors are expensive, have poor solubility, are prone to agglomerating when used, and many will significantly pollute the environment when used. Human environmental consciousness has grown as the founding of a sense of community with a shared future for humanity [15]. As a result, corrosion protection professionals now agree to use eco-friendly corrosion inhibitors. Amino acids, plant extracts, biological macromolecules, food tastes, and oral medications are typical environmentally friendly corrosion inhibitors. Plant extracts stand out among them for their benefits as corrosion inhibitors. Using plant extracts as corrosion inhibitors has the following benefits: a wide range of sources, renewable energy, environmental friendliness, and low cost. According to recent research on corrosion protection, numerous plants can be employed as inhibitors. In a 0.5 M H<sub>2</sub>SO<sub>4</sub> medium, the anti-corrosion mechanism of Veratrum root extract (VRE) for Cu was explored. According to electrochemical results, VRE has a 97% anti-corrosion capacity. With rising temperatures, veratrum root extract can still display significant levels of corrosion resistance [16]. The ability of Artemisia herba alba extract to prevent steel in hydrochloric acid media was discussed. The extract of Artemisia herba alba contains 0.4 g/L and has a 92% anti-corrosion efficiency [17]. Other researchers looked at the walnut fruit husk extract's ability to prevent corrosion in steel when exposed to a corrosive solution of 1 mol/L HCl. According to electrochemical findings, the anti-corrosion effectiveness of walnut fruit green husk extract is 95% when the concentration reaches 800 ppm [18]. Investigated was the ability of 5-(4-methoxyphenyl)-3-h-1, 2-dithiole-3-thione to suppress corrosion on copper in a 0.5 M sulfuric acid solution. The findings of the theoretical calculations and the experiments support the possibility of corrosion inhibition performance for 5-(4-methoxyphenyl)-3-h-1,2-dithiole-3-thione [19]. To prevent the corrosion of carbon steel, an aqueous extract of wild clary has been employed in place of a corrosion inhibitor. At a concentration of 20 mol/L and a temperature of 298 K, it exhibits a good inhibitory efficiency (IE) of 83.078% [20]. Apply the leaf extract of Falcaria vulgaris (FV) to reduce mild steel (MS) corrosion in a 1 M HCl environment. The polarisation results showed that when the ideal concentration of

800 ppm of FV leaf extract was added to the acid solution, the corrosion current density dropped from 264.0 A/cm<sup>2</sup> (for the sample submerged in the blank solution) to 20.4 A/cm<sup>2</sup>. After six hours of immersion, electrochemical impedance spectroscopy (EIS) measurements showed an inhibitory efficiency of 91.3% at this dose [21]. The anti-corrosion properties of oregano (*Origanum vulgare*) leaf essential oil for carbon steel in hydrochloric acid have been investigated. The maximum *O. vulgare* inhibition performance was discovered to be 85.64% at 2 g/l in 1 M HCl [22]. In addition to that, other studies have also used natural compounds extracted from seeds, fruits, and leaves to prevent the corrosion of metals and alloys [23–27]. Table 1 provides an overview of the literature evaluations and key characteristics [27–36]. In plant extracts, electronegative atoms, planar conjugate systems with different aromatic rings, and unsaturated bonds are present in numerous chemical compounds that include nitrogen, oxygen, phosphorus, and sulphur as primary constituents. The *Corchorus olitorius* plant is where some of these organic compounds can be located and harvested [37]. Egypt, Algeria, Lebanon, Nepal, Thailand, and many nations have *Corchorus olitorius* plants. While the rest of the plant, including the roots and stem, is typically thrown away as garbage. In Egypt, the leaves are used to prepare a traditional culinary dish. In this work, *Corchorus olitorius* stems from Egypt were treated with a warm water/ethanol solution to extract the organic material. The extract, collectively known as ECS, was utilised to prevent carbon steel corrosion in an aqueous solution of 1 M hydrochloric acid.

The objective of the current study was to assess the inhibitory effect of ECS as a green coating on carbon steel corrosion in a 1M HCl solution using a variety of techniques, including weight loss analysis, potentiodynamic, electrical frequency modulation, and impedance studies, thermodynamic parameters, and surface examination (FTIR, AFM, and XPS). The theoretical method involves simulations of molecular dynamics and quantum chemistry calculations

## 2. Materials and techniques

### 2.1. Chemicals

Hydrochloric acid was used to produce six molar, and the required concentrations were obtained by dilution with 37% HCl (rankem), and 0.1 M NaOH (rankem) was used in the experiment. Multiple

solutions having 1 M HCl were made using the produced HCl, either without or with various dosages of ECS ranging from 50 to 300 ppm.

The volume of the exam solution utilized in these investigations is 50 ml. They were prepared using non-ionized water. The temperature was regulated to 0.50 °C using a water thermostat.

## 2.2. The chemical conformation of ECS

The chemical composition of the stem has been extensively researched and well-recognized. Table 2 lists the most important types of sterols and fatty acids in *Corchorus olitorius* extract found in plants grown in Egypt [38, 39].

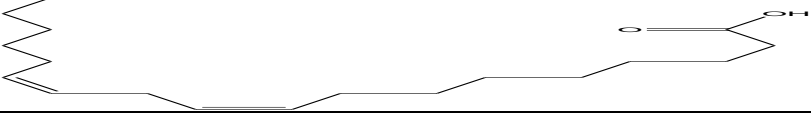
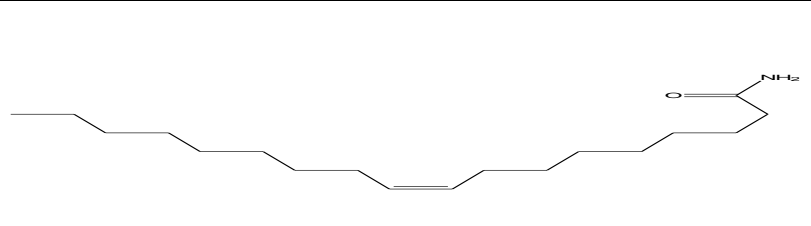
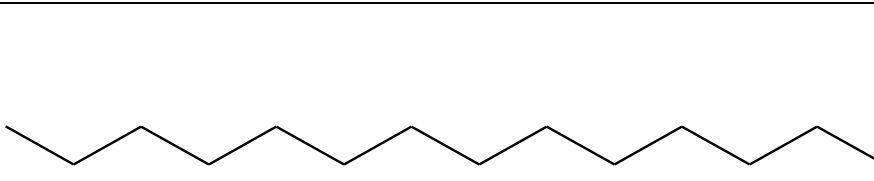
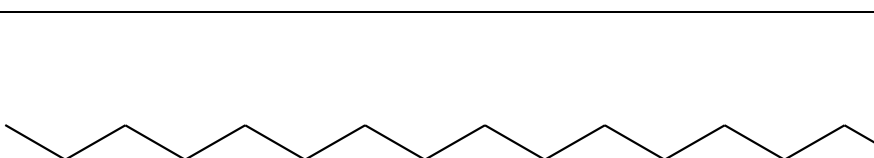
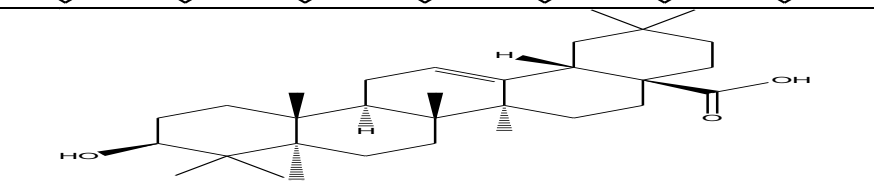
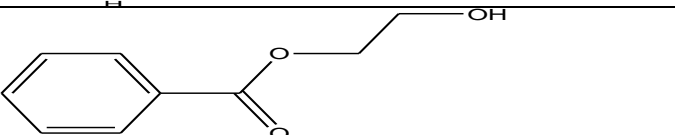
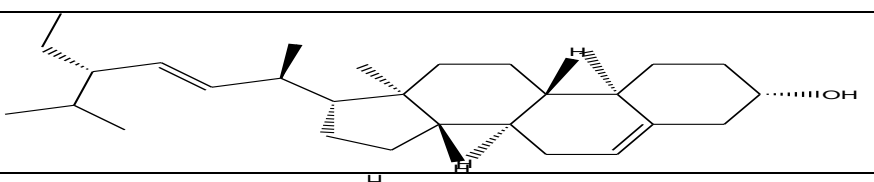
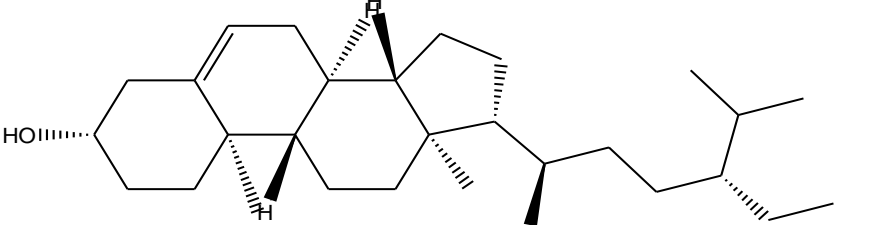
## 2.3. Preparation of an ECS inhibitor

Egypt's local supermarket is where I bought a fresh *Corchorus olitorius* plant. The stems (50 g) were divided and cleaned with deionized water. The stems are trimmed, dried, and then put in a grinder to be ground into powder. then treated with a 200-ml, v/v = 80/20 water/ethanol solution in a sealed bottle at 60 °C for eight hours. Following that, for 24 hours, the filtrate was maintained in a vacuum at 50 °C [12]. The acid was the corrosive medium. 1000 mL of water was applied to dilute 1 gram of the ECS to a concentration of 1000 ppm, and 1 M HCl was ready as a corrosive medium. Different volumes of ECS (1000 ppm) were taken from the stock solution to produce different concentrations of an extract with a corrosive medium.

**Table 1** steel corrosion inhibition by natural products

Plant extract	solutions	metals	%	References
<i>Olea europaea</i>	2MHCl	Carbon steel	93	25
<i>Cotula cinerea</i> , <i>Retama retam</i> , and <i>Artemisia herba</i>	2.3 M) sulphuric acid	X52 mild steel	67	26
<i>Rauvolfia serpentina</i>	1 M HCl and H <sub>2</sub> SO <sub>4</sub>	Mild steel	94	27
<i>Lupinus albus</i>	1 M HCl and H <sub>2</sub> SO <sub>4</sub>	steel	86.5	28
<i>Solanum tuberosum</i>	1M HCl and 1H <sub>2</sub> SO <sub>4</sub>	Mil steel	91.3	29
<i>Retama monosperma</i>	1M HCl	Carbon steel	83	29
<i>Olive leaves</i>	1M HCl	Carbon steel	93	30
<i>Eruca sativa seed extract</i>	1M HCl	Carbon steel	94.8	31
<i>Murraya koenigii</i>	1M HCl	Carbon steel	80	32
<i>ginger roots extract</i>	1MHCl	Carbon steel	94.9	33
<i>Black Tea</i>	1MHCl	Carbon steel	72	34

**Table 2** The constituents of the extract from ECS along with their names, formulas for molecular weights, structures [40,41].

Chemical structure	Name	Formula, MW,
<b>Fatty acids</b>		
	Linoleic acid	$C_{18}H_{32}O_2$ 280.45
	Oleic acid amide	$C_{18}H_{35}ON$ 281.48
	Palmitic acid	$C_{16}H_{32}O_2$ 256.42
	Stearic acid	$C_{18}H_{36}O_2$ 284.48
	Oleanolic acid	$C_{30}H_{48}O_3$ 456.36
	2-hydroxyethyl benzoate	$C_9H_{10}O_3$ 166.17
<b>Sterols</b>		
	Stigma sterol	$C_{29}H_{48}O$ 412.7
	$\beta$ -Sitosterol	$C_{29}H_{50}O$ 414.71

## 2.4. Preparation of samples

Carbon steel samples contain Si (0.002%), P (0.007%), C (0.200%), Mn (0.910%), and the remaining iron. Carbon steel pieces that measured 1x1x0.2 cm were used to assess weight loss (WL). The carbon steel sheet was polished at several grits (600, 800, 1000, and 1200) of sandpaper. The weight-loss experiment was carried out in compliance with ASTM guidelines [50]. After sanding, washing with double-distilled water, drying, and weighing the carbon steel coupons, ECS was added in quantities ranging from 50 ppm to 300 ppm. After being weighed, the samples are returned to their solutions. Up to the experiment's conclusion for 24 h, the stages are repeated every half-hour for the first (3 h), after (6 h), (12 h), and 24 h. All solutions prepared were 50 mL. The tests are conducted three times to obtain the most precise results; average values are calculated. The range of temperatures is 25 to 55 °C. The following formulas are used to determine inhibition efficiency (I.E.%) and corrosion rates (C.R.), respectively [42]:

$$C.R(\text{rate of corrosion}) = \Delta m/St.$$

(1)

$$\% IE = 1 - \left[ \frac{C.R_{inh}}{C.R_{Blank}} \right] = \theta \times 100$$

(2)

S stands for sample surface area in contact with the solution in cm<sup>2</sup>, m stands for mass decrease, and t stands for submersion period in min.

## 2.5. Examination of Potentiodynamic Polarization

Through the use of a cell made up of three conventional electrodes, including a working electrode made of carbon steel with a surface area of 1 cm<sup>2</sup> exposed to a corrosive solution and treated as before in the WL method, a reference electrode (SCE), and an auxiliary electrode (Pt foil), the potentiodynamic polarisation technique was used. The working electrode is submerged in the corrosive solution for 30 minutes to reach a steady state. Polarization curves were originally captured between -0.5 and 0.5 V at a constant scan rate of 0.1 mVs<sup>-1</sup> (SCE). Three times are repeated in an experiment to ensure repeatability. This is the inhibition efficiency that ECS has enabled [43]:

$$IE\% = \left[ i_{corr} - \frac{i_{corr(inh)}}{i_{corr}} \right] \times 100$$

(3)

$$\theta = \left[ i_{corr} - \frac{i_{corr(inh)}}{i_{corr}} \right]$$

(4)

$i_{corr}$  and  $i_{corr(Inh)}$  are the corrosion current density values in the absence and presence of ECS. These values were

determined by extrapolating both Tafel lines to the corrosion potential.

## 2.6. EIS (Electrochemical Impedance Spectroscopy) investigation

This technique made use of the same cell as the potentiodynamic polarisation strategy. The studies apply potential circuits and AC signals with peak amplitudes of 10 mV at frequencies between 100 kHz and 0.1 Hz (OCP). All EIS results agree with the proper equivalent circuit using the Gamry Echem software and the charge transfer resistance as a function of knowing the level of protection using the following equation [44].

$$IE\% = \left( 1 - \frac{R_{ct}}{R_{ct}^0} \right) \times 100$$

(5)

$R_{ct}$  and  $R_{ct}^0$ , the resistance of charge transfer with and without inhibitor respectively.

## 2.7. EFM (Electrochemical Frequency Modulation) Research

The signal with a size of 10 mV was applied during the EFM studies using two sinus waves with a frequency range of 2 to 5 Hz, and the decision was made based on three factors [45]. This technique is a fast and non-destructive technology. Through the higher peaks, the corrosion current density ( $i_{corr}$ ), causal factors (CF-2 and CF-3), and Tafel slopes ( $\beta_a$  and  $\beta_c$ ) were identified [46]. Gamry Potentiostat/Galvanostat/ZRA (PCI4-G750) was the instrument utilized in the EFM experiments in an electrochemical investigation. Gamry includes the DC105 corrosion program, the EIS300 EIS program, and the EFM140 program as a computer for data collection. Data were plotted, computed, and gathered using Echem Analyst 5.5. At 25 °C, solely electrochemical investigations were done.

## 2.8. The Surface Examination

Carbon steel samples were handled similarly to weight-loss samples in the previous section using carbon steel sheets that were 1 x 1 x 0.2 cm in size. The carbon steel pieces were subsequently polished with sandpaper in grades 600, 800, 1000, and 1200. The components were cleaned with filtered water, stripped off with acetone, and dehydrated as previously indicated [47].

### 2.8.1. Examination using Atomic Force Microscopy (AFM)

Atomic force spectroscopy (AFM) was used to examine the morphological properties of the carbon

steel surface. In the absence of ECS and the event of the maximum concentration of ECS (300 ppm), this examination is conducted in 1 molar of hydrochloric acid. Contact AFM was applied using a silicon nitride probe (MLCT model; Bruker). Software IP 2.1 was used to analyse the images., The scanning settings were tracked using the Proscan program 1.8.

### 2.8.2. Analysis using X-Ray Photoelectron Spectroscopy (XPS)

Electronic X-ray spectroscopy (XPS) was used in this study to test the morphology of carbon steel coupons before and after submerging in a solution of 1 M hydrochloric acid in the presence and absence of ECS (300 ppm) for 24 h. Measurements were taken using the ESCALAB 250Xi, made by Thermo-Scientific in the USA. Carbon steel samples were handled in the same treatment coupons from earlier sessions' weight loss method.

### 2.8.3. Analysis of Fourier Transform Infrared (FTIR) Spectroscopy

After adding ECS at a concentration of 300 ppm in a solution of 1 M HCl without dipping the carbon steel sample and in 1M HCl after a day of carbon steel dipping, the efficient groups in the ECS were determined using the FTIR technique and FTIR investigation through (FT/IR-4100typeASerial B117761016).

### 2.9. Computing using quantum chemistry

We investigated molecules using the Material Studio DMol3 module (version 7.0). A core group of double-digit polarization (DNP) and Becke One substitutable relationship functions (BOP) were added to the well-liked gradient method (GGA) in the DMol3 unit, and solvent effects were controlled via COSMO control. As mentioned in the equations below, the technique was utilised to locate specific chemical features such as electronegativity ( $-\chi$ , chemical potentials (Pi), fineness ( $\sigma$ ), and global solidity ( $\eta$ ) [48, 49].

$$Pi = -\chi \quad (6)$$

$$Pi = \frac{E_{LUMO} + E_{HOMO}}{2} \quad (7)$$

$$\eta = \frac{\Delta E}{2} = \frac{E_{LUMO} - E_{HOMO}}{2} \quad (8)$$

Universal hardness determines softness:

$$\sigma = \frac{1}{\eta}$$

(9)

Using the following equation and the parameters of global solidity and electronegativity, we determined the proportion of transported electrons ( $\Delta N$ ):

$$\Delta N = \frac{\chi_{Fe} - \chi_{inh}}{2(\eta_{inh} + \eta_{Fe})} \quad (10)$$

The absolute electronegativity data for the alloy and the inhibitory extract from ECS are denoted by the symbols  $\chi_{Fe}$  and  $\chi_{inh}$ , respectively. The measurements for iron's electronegativity are  $4.28 \text{ V mol}^{-1}$ , and its solidity is zero volt/ mol., individually, as said by multiple publications [50,51]. Using Fukui function accounting, a molecule's local reactivity was also finished. The primary targets for electrophilic and nucleophilic attacks by chemicals of ECS, respectively, are Fukui<sup>+</sup> and Fukui<sup>-</sup>.

### 2.10. Monte Carlo experiments

Monte Carlo simulations were used to achieve the interaction between the Fe (110) plane surface and the ECS inhibitor. The adsorption locator module from Biovia-Accelerys Inc.'s Material Studio 7.0 programme was used in this simulation [52]. In this work, the maximum steady Fe (110) plane was chosen to simulate the surface of carbon steel. This work mimicked the surface of carbon steel by using the top steady Fe (110) plane. Fe (110) was continued with periodic boundary positions using a box simulation of ( $32.27\text{Å}^0$ ,  $32.27\text{Å}^0$ , and  $50.18\text{Å}^0$ ) to imitate a standard part of the interface and prevent any arbitrary border impacts. The Forcite classical simulation engine was also used for the optimisation of energy. When the alloy surface (110) was first shaped, its surface area, supercell structure, and periodicity were changed. The plurality of the space, which at the time had a density of  $20\text{Å}^0$ , was constructed on the Fe (110) surface [53]. The layer function Object [native code] } first minimises the Fe (110) surface before designing the corrosion arrangement with the new inhibitor molecules. The potential for the adsorption of the novel molecules on the surface of the Fe (110) plane was modelled using the condensed phase optimised molecular potential for atomistic simulation studies force field (COMPASS). To identify the lowest-energy adsorption spots and their effects on the effectiveness of inhibition, corrosion-inhibiting ECS molecules were modelled on the Fe (110) surface [54].

### 3. A discussion of the findings

#### 3.1. Measurements of weight loss

##### 3.1.1. The influence of inhibitor concentration

To evaluate the inhibitory effect of ECS on steel corrosion, weight loss at 298 K following 24 h of immersion was used (Tables S1–S4). Fig. 1 depicts the influence of different ECS concentrations on corrosion rate and inhibition efficiency. ECS prevented the corrosion of carbon steel in 1 M hydrochloric acid. At 298K, raising the concentration of ECS reduces the corrosion rate. At 300 ppm and 298K, the inhibition

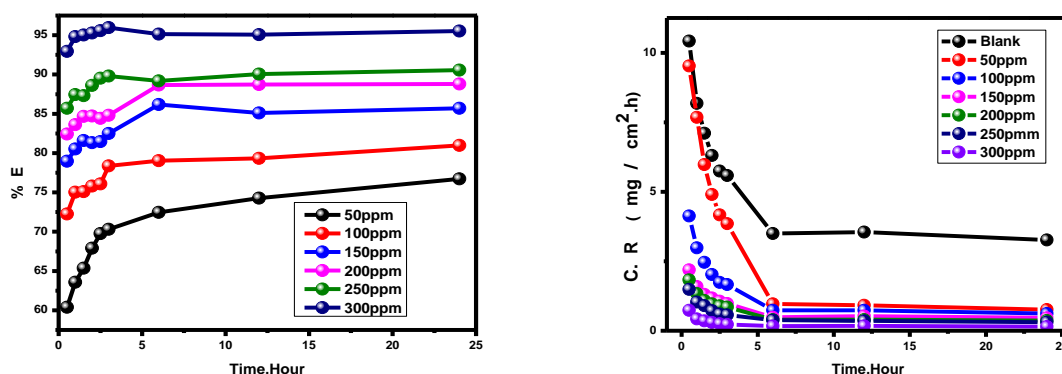


Fig.1: The carbon steel electrode's corrosion rate and inhibition effectiveness following an immersion time(0.5-24h) in a 1 M hydrochloric acid at 25 °C, both with and without varying ECS concentrations (50-300 ppm).

##### 3.1.2. The influence of contact time

Some authors suggest that in corrosion testing, the best scenario should be achieved by simulating real-world conditions by reproducing a favourable processing environment [62]. It has been emphasised that 6 to 8-hour HCl stimulation sessions are typical [63]. While some studies have shown that investigations within 4–48 hours can yield reliable data regarding the rate of corrosion in HCl [64], most studies now find that a 24-hour test is more feasible and typical.

##### 3.1.3. Temperature influence

The effectiveness of corrosion inhibition and the adsorption of the inhibitor on the metal surface are both significantly influenced by temperature [65–68].

efficiency increased to 95.53%. Corrosion inhibition can be explained by the fact that ECS contains different organic compounds with diverse functional groups and heteroatoms, aromatic rings, and conjugated double bonds that form a protective coating on the metal surface after adsorbing [55–57]. The ECS's abundance of chemicals also suggests intramolecular synergy through the cooperative adsorption of the functional groups in the extract. Adsorption on the metal surface occurs through favourable contact [58–61].

Corrosion happens more quickly as the temperature rises. In fact, at 300 ppm concentration, the corrosion rate at 298 K temperature was  $0.005881 \text{ mg cm}^{-2} \text{ min}^{-1}$  and  $0.114944 \text{ mg cm}^{-2} \text{ min}^{-1}$  at 328 K temperature. At 328 K, the inhibition efficiency for 300 ppm dropped from 95.03% at 298 K to 81.71%. Fig.2. This modification shows that when the temperature rises between the inhibitory molecules and the carbon steel surface, there is a balance between adsorption and desorption (Tables S1 and S2). This equilibrium leans in the direction of desorption [69–71]. This implies that the ECS molecules may adhere to the metal surface and that temperature affects how the ECS interacts with the carbon steel. Figs. S1–S12 demonstrate the effect of different temperatures on inhibition efficiency, weight loss, and corrosion rate.

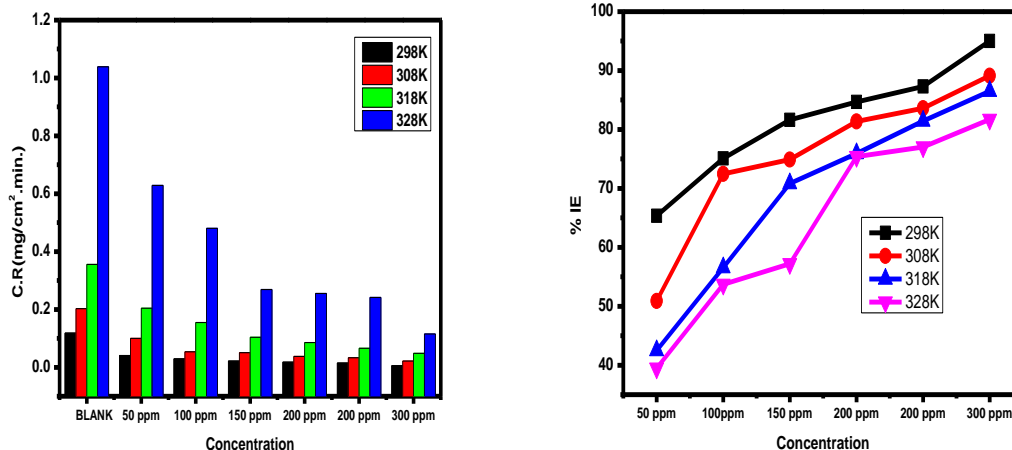


**Fig.2:** The carbon steel electrode's corrosion rate and inhibition effectiveness following a 90(min.) immersion in a 1 M hydrochloric acid at various temperatures (25-55 °C), both with and without varying ECS concentrations (50-300 ppm). [

### 3.1.4. kinetic and thermodynamic parameters

The Arrhenius equation (11) [72-75] determines the link between the activation energy and the rate of corrosion in a corrosion reaction, and the standard enthalpy ( $\Delta H^*$ ) and activation entropy ( $\Delta S^*$ ) are obtained from the transition state equation.

$$\log(C.R) = \left( \frac{-E_a^*}{2.303RT} \right) + \log A \quad (11)$$

$$\log C.R = \frac{\Delta S^*}{2.303R} - \frac{\Delta H^*}{2.303RT} + \log \left( \frac{R}{Nh} \right) \quad (12)$$

The Avogadro number, Plank constant, apparent activation entropy, pre-exponential factor, apparent activation energy, and activation enthalpy are all represented by the following formulas:  $\Delta S^*$  = apparent activation entropy,  $\Delta H^*$  = activation enthalpy,  $N$  = Avogadro number, pre-exponential factor =  $A$ , and apparent activation energy = ( $E_a^*$ ). Arrhenius plots produced in the presence of various extract concentrations and in the presence of a 1 molar HCl medium are shown in Fig. 3. By performing a linear regression on  $\log(C.R)$  and  $\log(C.R/T)$  as functions of  $1000/T$ , the  $E_a^*$ ,  $\Delta H^*$ , and  $\Delta S^*$  were considered. Table 3 shows the thermodynamic variables. The slope of  $\log(C.R.)$  about  $1000/T$  is represented by the values of  $E_a^*$  multiplied by  $(2.303 \times \text{perfect gas constant})$ . The  $\Delta H^*$  is estimated from its slope multiplied by  $(2.303 \times \text{perfect gas constant})$ , and the  $\Delta S^*$  is derived from the intercept of  $\log(C.R/T)$  relative to  $1000/T$  (Fig. 4) [76]. These findings suggested that the inhibitor physisorption adsorption is adsorbed on the metal surface since the  $E_a^*$  obtained in the presence of ECS is more than 1 M hydrochloric acid [86]. The rise in

$E_a^*$  with ECS concentration is viewed as an electrostatic metal's inhibiting response, which forms a physical barrier. The controlled solution had a higher activation energy than the uncontrolled solution. These results are consistent with earlier studies [77–83]. Pre-exponential factor ( $A$ ) variance in both acids was discovered to be comparable to visible activation energy variation (see Fig. 5). Other investigations found results that were similar to these [84–86]. The current investigation demonstrated a relationship between more apparent activation energy and more pre-exponential variables, whereas a relationship between lower pre-exponential factors and lower activation energies was discovered. The tested inhibitor met its aims by preventing corrosion even at low corrosion activation energies. Because all  $E_a^*$  values in both acids exceed comparable  $\Delta H^*$  values, a gaseous reaction, such as hydrogen evaporation, occurs throughout the corrosion process. Additionally,  $RT$ 's average is almost the same as the moderate discrepancy between activation energy and enthalpy. Additionally, the corrosion development is an unimolecular reaction, as stated by equation (13) because the half value of the variation amongst activation energy and enthalpy is almost equivalent to the intermediate value of  $RT$ , where  $T$  is a temperature in the investigational temperature variety [87]:

$$E_a^* - \Delta H^* = RT \quad (13)$$

Positive  $\Delta H^*$  values indicate endothermic adsorption. [88-90]. Metal dissolution decreases when ECS concentrations grow due to an increase in  $\Delta H^*$ . The more ECS there is, the more positive the sign of



DS\* becomes. The active complexes produced are less ordered, indicating that the corrosion reaction media are less ordered since ECS molecules are present [91–93]. The  $\Delta E^*$  and  $\Delta H^*$  values increased dramatically when ECS particles (50 ppm) were counted in the corrosive medium compared to the uncontrolled solution, rising from 5.877 to 66.88 kJ/mol. and 5.677

to 64.38 kJ/mol., respectively. These results imply that the addition of ECS particles to the corrosion medium induces an inhibitory film to form as a shield on the surface of the alloy, resulting in an energy fence for the corrosion process compared to the unfettered solution and reducing the corrosion rate.

**Table 3:** The thermodynamic activation parameters for carbon steel corrosion in 1 M HCl in the presence and absence of ECS at various concentrations.

Inhibitor conc.(ppm)	$E_a$ K.J mol <sup>-1</sup>	$\Delta H^*$ K.J mol <sup>-1</sup>	$-\Delta S^*$ J mol <sup>-1</sup> k <sup>-1</sup>	log A
blank	5.877	5.677	197.03	0.9237
50	66.88	64.38	138.10	10.64
100	70.9	68.30	133.44	10.65
150	72.18	69.64	131.14	10.92
200	72.97	70.73	128.37	11.25
250	76.29	73.70	124.95	11.66
300	78.79	76.37	124.07	11.76

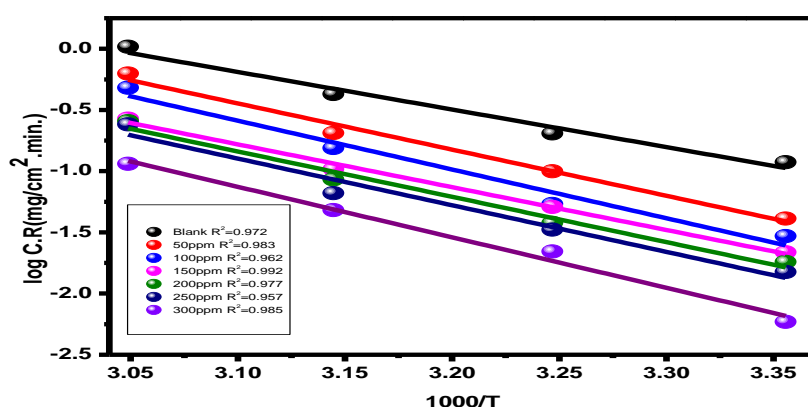


Fig. 3: Arrhenius curves for carbon steel in 1 M HCl with and without quantities of ECS (log C.R against 1000/T).

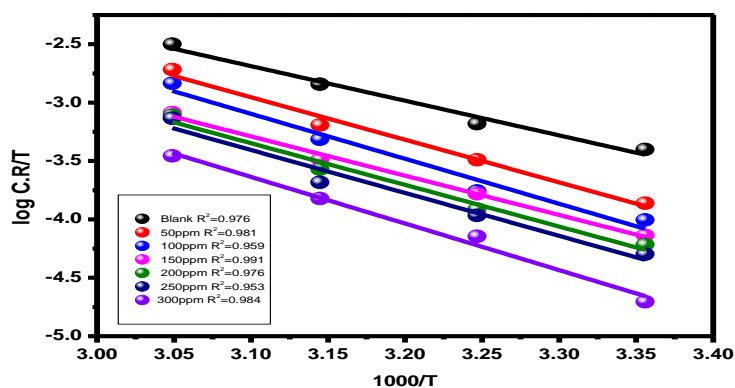


Fig. 4: Shows the transition states of alloy electrodes in a 1 M hydrochloric acid with varying concentrations of the ECS.

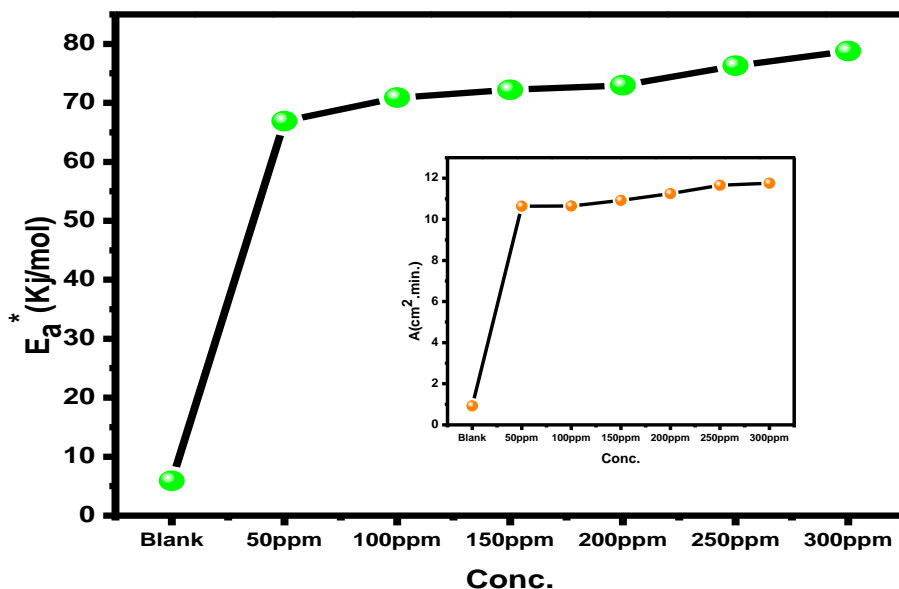
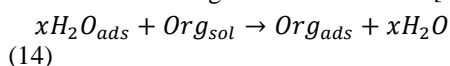


Fig.5: The relationship between E\*a and A with various doses of ECS at 1 M HCl.

### 3.1.5. Adsorption research

Because the binding energy between the water particles and the outside surface is lower than that between the particles of the inhibitor and the metal's surface, the ECS inhibitor has shown through adsorption on its surface that it can prevent carbon steel from oxidising in corrosive media [94].



Where x represents the number of single organic particles used in place of water molecules, particles of metal can be physisorbed or chemisorb; the physisorbed molecules combat metal corrosion by reducing the cathodic riposte, while the chemisorbed particles obstruct the anodic response by lowering the potential reaction of the corroding alloy at the sites of adsorption [95]. The observed ECS's adsorption activity on the surface of carbon steel can be modelled using the adsorption isotherm. Using data from weight loss tests, we chose the best adsorption isotherm to describe the adsorption mechanism of ECS on the alloy surface in acidic environments [96–101]. In our circumstances, Langmuir and Temkin adsorption isotherms were discovered to be the optimal isotherms for the adsorption process (equations 15 and 16) and (Figs. S13–S18 and Figs. 6 and 7).

$$\frac{C}{\theta} = \frac{1}{K_{ads}} + C_{inh} \quad (15)$$

where C represents the concentration of ECS and  $K_{ads}$  is the adsorption equilibrium constant.

$$a\theta = \ln K_{ads} C \quad (16)$$

$K_{ads}$  is the equilibrium adsorption constant, (a) is a molecular interaction parameter, and C is the concentration of ECS, respectively.

Specifically, the binding force of the alloy surface of the inhibitor particles is shown by the  $K_{ads}$  value, which also represents the potency of the adsorption force between the alloy surface and the ECS molecules. The Big  $K_{ads}$  value, for instance, means that the ECS particles cling to the alloy surface more powerfully. It demonstrated that the equilibrium constant was higher than in previous research [102, 103]. It was found that Langmuir isotherms are more precise than Temkin isotherms in describing how ECS adheres to the surface of the alloy. The adsorption data of Gibbs free energy are determined using equation (17).

$$K_{ads} = \frac{1}{55.5} \exp\left(\frac{\Delta G_{ads}^0}{RT}\right) \quad (17)$$

The projected  $\Delta G^0_{ads}$  negative values are displayed in Table 4, proving that alloy spontaneity is

an exothermic operation that is temperature-dependent and allows the inhibitor to be adsorbed on the steel's surface as the reaction temperature rises [104]. In the duration of corrosion inhibition, chemisorption and physisorption are the two adsorption types that are widely discussed [105]. The electrostatic interaction between the negatively charged carbon surface and the charged molecules of the ECS is referred to as physical adsorption. Between 20 kJ/mol., and 40 kJ/mol With the reading heads set to 40, chemical adsorption often outweighs physical adsorption; however, at 40 kJ mol<sup>-1</sup>, there is simple chemical adsorption. Readings of  $\Delta G_{ads}^0$  up to 20 kJ mol<sup>-1</sup> are by physical adsorption [106]. Adsorption enthalpy ( $\Delta H_{ads}^0$ ) and entropy of

adsorption ( $\Delta S_{ads}^0$ ) are two thermodynamic adsorption parameters that can be intended using the combined form of the Van't Hoff equation (18) (Fig. 8) [107].

$$\ln K_{ads} = \left(-\frac{\Delta H_{ads}^0}{RT}\right) + \left(\frac{\Delta S_{ads}^0}{R}\right) + \ln\left(\frac{1}{55.5}\right) \quad (18)$$

The exothermic character of the adsorption of ECS on the alloy surface is designated by the negative sign of  $\Delta H_{ads}^0$ . Exothermic adsorption is connected with negative values of  $\Delta S_{ads}^0$ . This is consistent with the predicted outcome; even though adsorption is an exothermic procedure, it should be followed by a decline in entropy variation; even the opposite should occur [108].

**Table 4:** Langmuir and Temkin isotherms ( $K_{ads}$  and  $\Delta G_{ads}^0$ ) for different concentrations of ECS in 1 M HCl solution

Temp. °C	Langmuir isotherm					a	Temkin isotherm				
	$K_{ads}$	$R^2$	$-\Delta G_{ads}^0$	$-\Delta H_{ads}^0$	-		$K_{ads}$	$R^2$	$-\Delta G_{ads}^0$	$-\Delta H_{ads}^0$	-
	$\Delta S_{ads}^0$ J k <sup>-1</sup>		(K.J)	(K.J)			$\Delta S_{ads}^0$ J.k <sup>-1</sup>		(K.J)	(K.J)	
25	28.986	0.991	18.27	28.5	34.2	4.12	3.21	0.965	12.84	27.14	45.7
35	21.39	0.994	18.13			4.02	3.11	0.932	13.19		
45	12.75	0.995	17.35			6.53	2.084	0.991	12.56		
55	10.72	0.959	17.42			5.09	1.129	0.934	11.28		

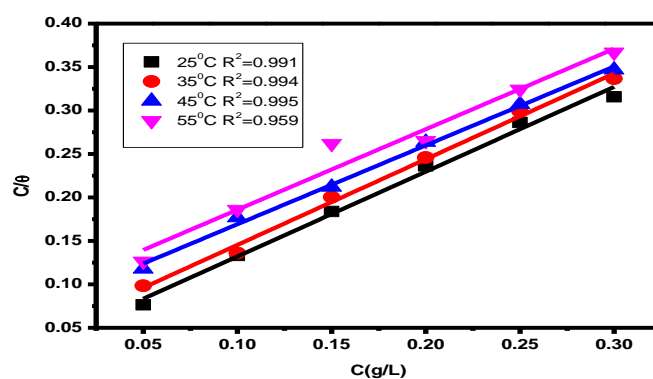


Fig.6: Langmuir adsorption isotherm of the extract of ECS for alloy corrosion in 1 M HCl solution at 25 °C as C/θ vs. log C.

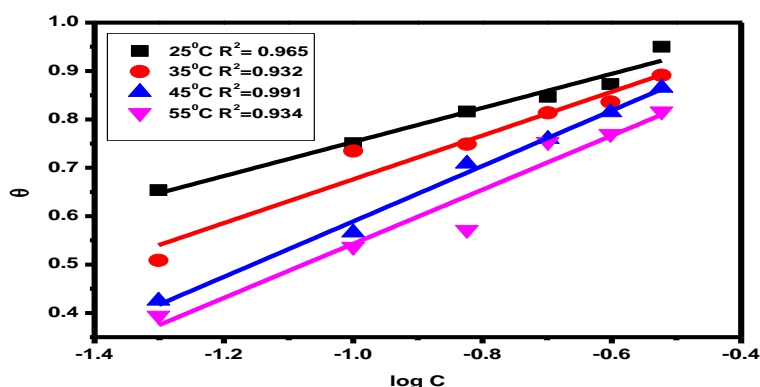


Fig.7: Temkin adsorption isotherm of the extract of ECS for alloy corrosion in 1 M HCl solution at 25 °C as  $\theta$  vs.  $\log C$ .

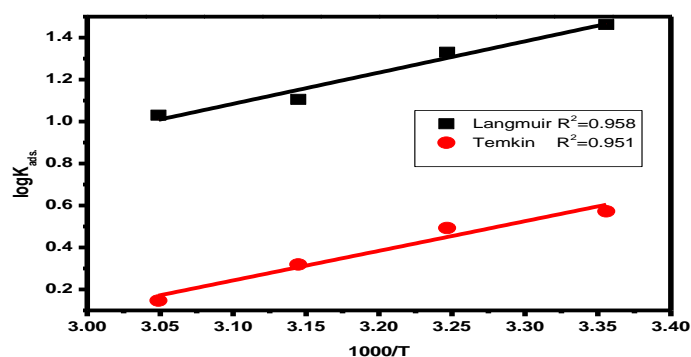


Fig.8: Equation for Van't Hoff (relation between absolute temperature and adsorption equilibrium constant).

### 3.1.6. The extract's anti-corrosion components

Previous research on pure synthetic or other organic compounds derived from natural resources allowed for the natural organic compounds listed in Table 2 to inhibit metal corrosion. Some metals, these pure chemicals, or their derivatives have affected corrosion inhibition. Various fatty acids have been reported to be effective, ecologically friendly stainless steel corrosion inhibitors [109]. Stearic acid and stearic imidazoline were used as corrosion inhibitors of iron in  $0.1 \text{ mol dm}^{-3} \text{ HClO}_4$  aqueous solutions, and the inhibition efficiency was 55% for stearic acid and 78.7% for stearic imidazoline [110]. Also, with an emphasis on long-term immersion testing, the synergistic inhibitory impact of stearic acid and (+)- $\alpha$ -tocopherol (E307) as a green inhibitor within a highly hydrophobic layer was explored on the corrosion of low-carbon, ferritic, and stainless steel, and the corrosion inhibition was 99.75% [111]. Linoleic acid's (LA) effectiveness at preventing corrosion of 1018 carbon steel in a  $0.5 \text{ M H}_2\text{SO}_4$  solution was assessed

using a combination of methods (including electrochemical research and a theoretical study). The corrosion inhibition arrived at 97% [112].  $\beta$ -Sitosterol, extracted from rice hulls, is a powerful mild steel corrosion inhibitor in  $1 \text{ M H}_2\text{SO}_4$ , with an efficiency of 76% [113]. With the aid of a microwave reactor, palmitic acid imidazole (PI) was created. The obtained product was investigated to determine the mild steel's ability to prevent corrosion in  $1 \text{ mol. L}^{-1} \text{ H}_2\text{SO}_4$ . At ambient temperature, it provided the highest level of 90% inhibitory efficiency [114].

## 3.2. Electrochemical studies

### 3.2.1. Measurements of the open circuit potential (OCP)

The fluctuation of the alloy electrode's OCP over time in a  $1 \text{ M HCl}$  solution at  $25 \text{ }^\circ\text{C}$  in the presence and absence of various ECS concentrations is shown in Fig. 9. The concentrations of ECS increased, and a significant shift to higher positive values was identified in the OCP. This can be caused by the ECS molecules adhering to the alloy surface. Intriguingly,

as depicted in Fig. 9, the OCP versus time seems to stabilise more, indicating that, in contrast to the control experiment, there is a dynamic equilibrium between the inhibitor molecule's adsorption and desorption on

the steel surface [115]. The addition of the inhibitors to the corrosive medium has a powerful effect on the anodic response.

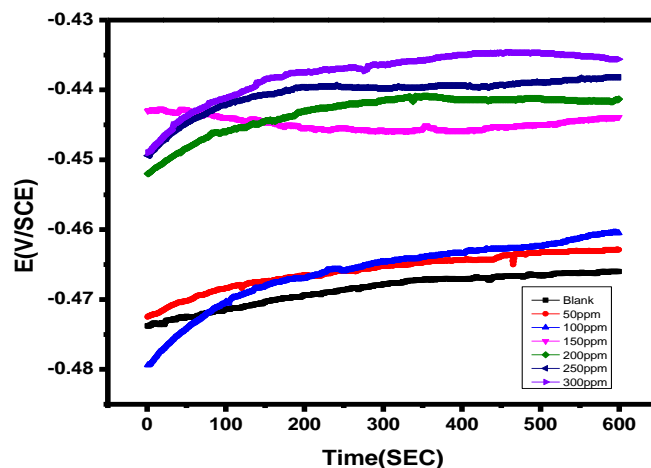


Fig.9: OCP potential-time curves for carbon steel in 1 M HCl when the ECS is absent or present at various concentrations.

### 3.2.2. Method of potentiodynamic polarization

A carbon steel electrode was subjected to anodic and cathodic polarisation in a 1 M HCl solution with and without varying amounts of the ECS at 25 °C (see Fig. 10). Important electrochemical parameters, such as current density of corrosion ( $i_{corr}$ ), corrosion potential ( $E_{corr}$ ), cathodic ( $\beta_c$ ) and anodic ( $\beta_a$ ) Tafel slopes, the resistance of polarization ( $R_p$ ), corrosion rate (C.R), and inhibition efficiency (I.E%), are all represented by values in Table 5. These values were obtained from the polarization curves that correspond to these parameters. The results show that adding modest concentrations of 300 ppm of ECS caused the C.R. values to quickly drop from 234.32 of the uninhibited solution (blank) to 12.4 mpy. Only by adding a tiny concentration (300 ppm) of ECS did the  $E_{corr}$  move to a positive value due to the inhibitor molecules adhering to the metal surface. It's interesting to see that lowering the inhibitor concentrations causes the corrosion potential numbers to rise once again.  $E_{corr}$  statistics also show that the inhibitors under study exhibit mixed-type inhibitor behaviour because of the minimal volatility in the acquired  $E_{corr}$  values [116]. Potentiodynamic polarization experiments demonstrate that the anodic and cathodic curves of corrosion current density ( $i_{corr}$ )

have substantially changed to lower values in the presence of inhibitor molecules. Because ECS slows down the anodic and cathodic processes of the steel electrodes, corrosion rates (C.R.) dropped, but percentage inhibition potency (I.E.%) rose. When it was introduced to the corrosion medium of 1M HCl, ECS had a maximum I.E. of 95.5% in a 1 M HCl solution at a concentration of 300 ppm. When the inhibitor concentrations were changed, the values of the Tafel slopes only slightly changed, demonstrating that the dissolution process is still carried out by anodic metal dissolution and cathodic hydrogen evolution [117]. It is still unclear why the corrosion potential readings went more negative again when inhibitor doses increased. The most likely explanation for this is that the ECS inhibitor influences the hydrogen evolution and oxygen reduction processes of alloys, raising alloy surface resistance and generating selective precipitation on the surface of the iron.

Another intriguing finding was a strong correlation between the Tafel polarisation results and the examinations of weight loss. Because of the extract's adsorption on the surface of the carbon steel, as seen in Fig. 11, increasing the concentration of ECS increased the polarisation resistance [118].

**Table 5** displays the impact of the concentration of ECS on the variables used in experiments using the potentiodynamic method to measure the alloy corrosion in 1 M HCl at 25 °C.

Conc.,ppm	$-E_{\text{corr}}$ , mV vs. SCE	$R_p$ , ohm	$i_{\text{corr}}$ , $\mu\text{A}\cdot\text{cm}^{-2}$	$\beta_a$ , $\text{mV}\cdot\text{dec}^{-1}$	$-\beta_c$ $\text{mV}\cdot\text{dec}^{-1}$	$\theta$	$\pm\%I.E$
blank	497±2	7.36±0.2	690±8	159.4±2	208.2±3	-----	----
50	425±4	14.67±0.1	230.3±3	85.2±3	170.8±2	0.666	66.6
100	432±5	15.32±0.1	157.2±2	79.2±1	149.3±2	0.772	77.2
150	439±2	18.23±0.3	129.2±2	78.5±3	137.2±3	0.813	81.3
200	444±4	19.69±0.2	106.4±1	78±2	132±1	0.845	84.5
250	455±3	21.45±0.3	87.2±0.5	76.5±1	129.9±2	0.873	87.3
300	467±6	23.78±0.1	31.3±0.3	70.7±3	118.7±1	0.954	95.5

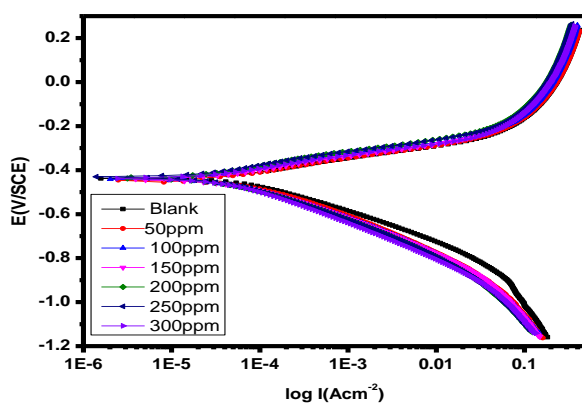


Fig.10: Corrosion of carbon steel in 1 M HCl in the absence and presence of various amounts of ECS.

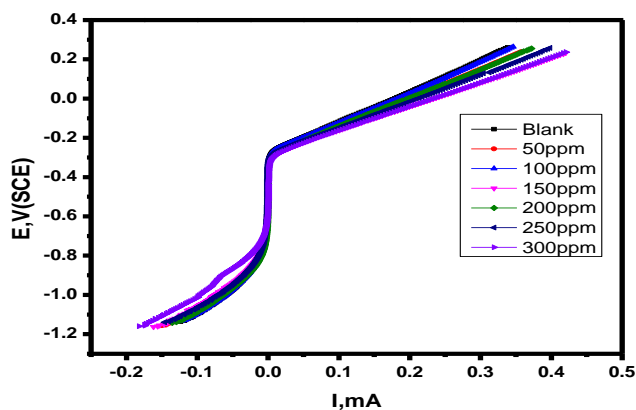


Fig.11: The carbon in 1 M HCl displayed by linear sweep voltammetry using various doses of the ECS.

### 3.2.3. Electrochemical Impedance Spectroscopy (EIS)

The electrochemical changes at the metal/electrolyte interface can be observed in real time using EIS. It is a good technique for understanding physical processes and gaining new knowledge [119, 120]. The environment around the carbon steel/electrolyte contact is complex, and it has two lines, each of which includes an ion, one of which is positively charged and the other is negatively charged. As a result, the ions that diffuse into the metal surface and the charges that travel in and out of it generate a range of impedances in the oxide layer that covers the surface of the alloy electrode. Additionally, the oxide coating contains capacitance caused by the electrical double layer  $C_{dl}$ , the resistance of charge transfer ( $R_{ct}$ ), and the resistance of solution ( $R_s$ ). Table 6 provides an overview of the EIS parameters obtained for carbon steel electrodes immersed in 1 M HCl and varying doses of ECS corrosion inhibitor at 25 °C. Figs. 12 and 13 show that the Nyquist and Bode plots were produced when various ECS concentrations were present. Due to higher charge transfer resistance, increasing the concentration of ECS causes the semicircle's diameter to rise during the corrosion process [130]. As a result, the chosen corrosion inhibitors are adsorbed at the electrolyte/metal interface, increasing corrosion resistance and lowering the corrosion rate. Referring back to Table 6, it can be observed that adding the concentration of ECS (300 ppm) significantly reduces the  $C_{dl}$  values compared to what they would have been in the bulk solution. Inhibitor molecules are adsorbed at the electrolyte/metal interface, which results in a thicker electric double layer or a lower local dielectric constant [121, 122]. The impedance diagram, which has a practically semicircular shape, illustrates the charge transfer mechanism that regulates carbon steel corrosion. The Bode graphs of carbon steel soaked in 1 M HCl are shown in Fig. 13 in the absence and presence of various ECS concentrations. The impedance modulus for the blank solution is enhanced by 1-2 orders of magnitude in the low-frequency region, as seen in Fig. 13. The impedance modulus increases more visibly with ECS. Also, in the broad frequency range of the middle, the phase angle value is close to 90, and the slope of  $\log |Z|$  and  $\log f$  is close to -1. This shows the carbon steel surface generates perfect capacitive behaviour [123]. Due to the overlap of the two peaks in the phase angle plots, the phase angle diagram becomes noticeably broader as ECS

concentration rises. As a result, it may be concluded that two time constants are produced, one of which is a result of the electric double-layer capacitance ( $C_{dl}$ ) at the metal/solution interface. Another factor contributing to the relaxation process at the carbon steel/solution contact is the adsorption and desorption of ECS [124]. The more the ECS adsorbs the carbon steel surface, the broader the phase angle maps are. The equivalent circuit that the EIS data is simulated through is shown in Fig. 14. This circuit was chosen because it mimics various non-homogeneities without the need for capacitors by using CPE (constant-phase elements), including grain boundaries, surface roughness, and surface contaminants in steel. The following equation [125] can be used to represent frequency, which is a significant factor in element impedance:

$$Z_{CPE} = (j\omega)^{n-1} Y_0^{-1} \quad (19)$$

$Y_0^{-1}$  is the CPE value,  $j^2$  is an imaginary number equivalent to (-1) and stands for the sine wave modulation angular frequency ( $\omega = 2\pi f$ ;  $f =$  ac frequency). The identical circuit's quality was evaluated using the chi-square value [126]. Table 6 demonstrates that the accepted chi-square data (0.00017 to 0.00022) pinpoints a good fit for the suggested circuit. Because of the influence of numerous parameters, including surface electrode roughness, heterogeneity of the surface, and the dielectric constant, the magnitude of  $n$  in total experimental settings ranges from 0 to 1.

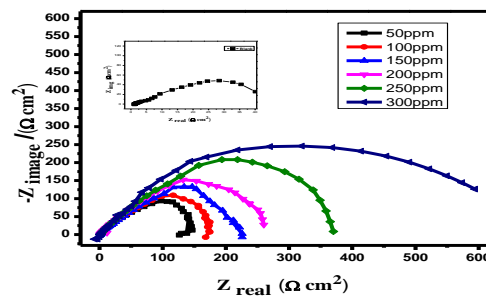
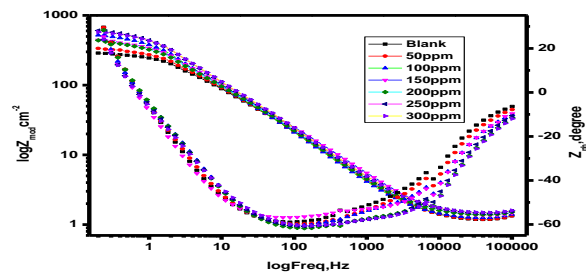
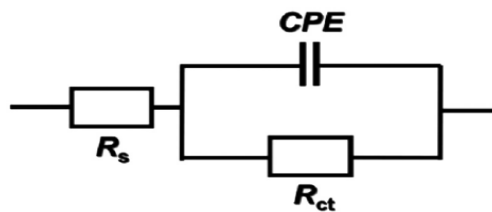
The  $n$  value of 1M HCl alone is high in our study compared to the inhibition system. When the ECS concentration increases, the rate drops, demonstrating that the surface of the alloy is reasonably homogeneous and the inhibitor adsorption is not uniform [136]. The double-layer capacitance ( $C_{dl}$ ) was estimated using the following equation [127, 128].

$$C_{dl} = Y_0 \omega^{n-1} / \sin\left[n\left(\frac{\pi}{2}\right)\right] \quad (20)$$

Intriguingly, the findings from the EIS data were in good accord with those from measurements of potentiodynamic polarization and weight loss. ECS was used to achieve a maximum I.E. of 94.2% at a concentration of 300 ppm in a 1 M HCl solution.

**Table 6:** The outcomes of the EIS method for corrosion of alloy at 25°C in 1 molar hydrochloric acid with varying amounts of extract from ECS.

Conc., (ppm)	$R_{ct}$ , $\Omega \text{ cm}^{-2}$	$R_s$ , $\Omega \cdot \text{cm}^{-2}$	$Y^0 \times 10^6$ , $\mu\Omega^{-1} \text{ S}^n \text{ cm}^{-2}$	$n \times 10^3$	$C_{dl} \times 10^4$ , $\text{F cm}^{-2}$	$\theta$	IE% <sub>EIS</sub>	$\chi^2$
Blank	40.2±0.03	1.27±0.014	433.0±2.2	841±3.6	2.27	-----	-----	0.00017
50	130.3±1.3	1.195±0.014	421.0±2.1	773±2.8	1.54	0.689	68.9	0.00019
100	176.9±1.4	1.16±0.013	411.8±1.9	753.6±2.9	1.49	0.772	77.2	0.00018
150	220.3±2.1	1.36±0.015	407.8±1.7	744.8±2.4	1.30	0.817	81.7	0.00013
200	264.5±2.2	1.38±0.012	400.0±1.8	737.3±1.9	1.11	0.848	84.8	0.00014
250	355.5±2.4	1.084±0.011	365.5±1.9	723.1±1.8	0.987	0.886	88.6	0.00020
300	700.5±3.2	1.063±0.012	345.2±2.3	717.3±1.9	0.789	0.942	94.2	0.00022

**Fig.12:** Nyquist plots for the corrosion of carbon steel at 1 M HCl in the presence and absence of various amounts of ECS.**Fig.13:** Bode graphs showing the carbon steel corrosion at (1) molar hydrochloric acid in the absence and presence of various quantities of ECS at 25 °C.**Fig.14:** Typical of an analogous circuit for computing EIS information.



### 3.2.4. Electrochemical frequency modulation technique (EFM)

Given that EFM has a lot of benefits, including rapid testing and corrosion current values that are delivered without the requirement for prior Tafel constant information, also the reality that it isn't destructive, it is utilized in this job [129]. Similar to EIS, this technique also uses a short AC signal, only it also features two sine waves that can be applied to the cell simultaneously, individually it containing a distinct frequency. Because of the current's non-linear connection to the potential excitation in this technique, the input frequencies are included in the current response. This method's input frequency is the total, multiples, and differences of two input frequencies. Minuscule frequencies that increase an integer from the fundamental frequency, which determines the experiment's duration, are essential. Table 7 displays the EFM corrosion characteristics for carbon Eq.21 was used to compute the inhibitory efficiency percentage (I. E %).

$$IE\% = \frac{[i_{EFM} - i_{EFM(inh)}]}{i_{EFM}} \times 100 \quad (21)$$

To internally verify the validity of the EFM strategy, the abbreviations CF-2 and CF-3 are utilized [130]. CF-2 and CF-3 typically have values of 2 and 3, respectively. Because the causal components in this scenario deviate significantly from the expected values, noise distorts the measurements. Another cause for the inadequate effectiveness of the inhibitor is a variation of the causative factors from their ideal values, which can happen when either the resolution of the frequency spectrum is insufficient or/and the inactivation amplitude is too modest [131,132]. Data on causation factors are included in Table 7, and it is evident that the measured values are of the highest possible calibre. The intermodulation spectrum is a spectrum of the current response as a function of frequency, and it is used to illustrate the outcomes of the EFM experiment. ECS was used to record the intermodulation spectrum of an alloy electrode in a solution of 1 M HCl, both in the absence and presence of various doses, as shown in Fig.15. The outcomes are totally in line with those from Tafel polarization, EIS, and weight loss studies.

**Table 7.** The EFM technique was used to measure the electrochemical carbon steel parameters in 1 M HCl in the absence and presence of various concentrations of ECS at 25 °C.

Conc., ppm	$i_{corr}$ , $\mu A cm^{-2}$	$\beta_a$ , $mV dec^{-1}$	$-\beta_c$ , $mV dec^{-1}$	CF-2	CF-3	$\theta$	I.E%	C.R mpy
Blank	280.34±3	66.99±0.4	88.28±2	2.009±0.02	3.66±0.05	-----	-----	36.6
50	89.58±0.9	83.57±0.2	124.5±3	2.016±0.02	3.11±0.04	0.680	68.0	32.83
100	78.95±0.7	73.95±0.5	116.7±2	1.980±0.04	3.22±0.05	0.718	71.8	26.93
150	56.19±0.8	109.6±1.1	113.7±4	2.050±0.03	2.93±0.06	0.799	79.9	23.87
200	42.25±0.2	93.93±0.3	112.7±2	1.99±0.02	3.08±0.05	0.849	84.9	20.52
250	34.91±0.3	87.33±0.2	136.2±3	2.009±0.06	2.94±0.02	0.875	87.5	18.67
300	17.24±0.4	79.57±0.4	115.1±2	1.87±0.03	3.03±0.03	0.938	93.8	15.94

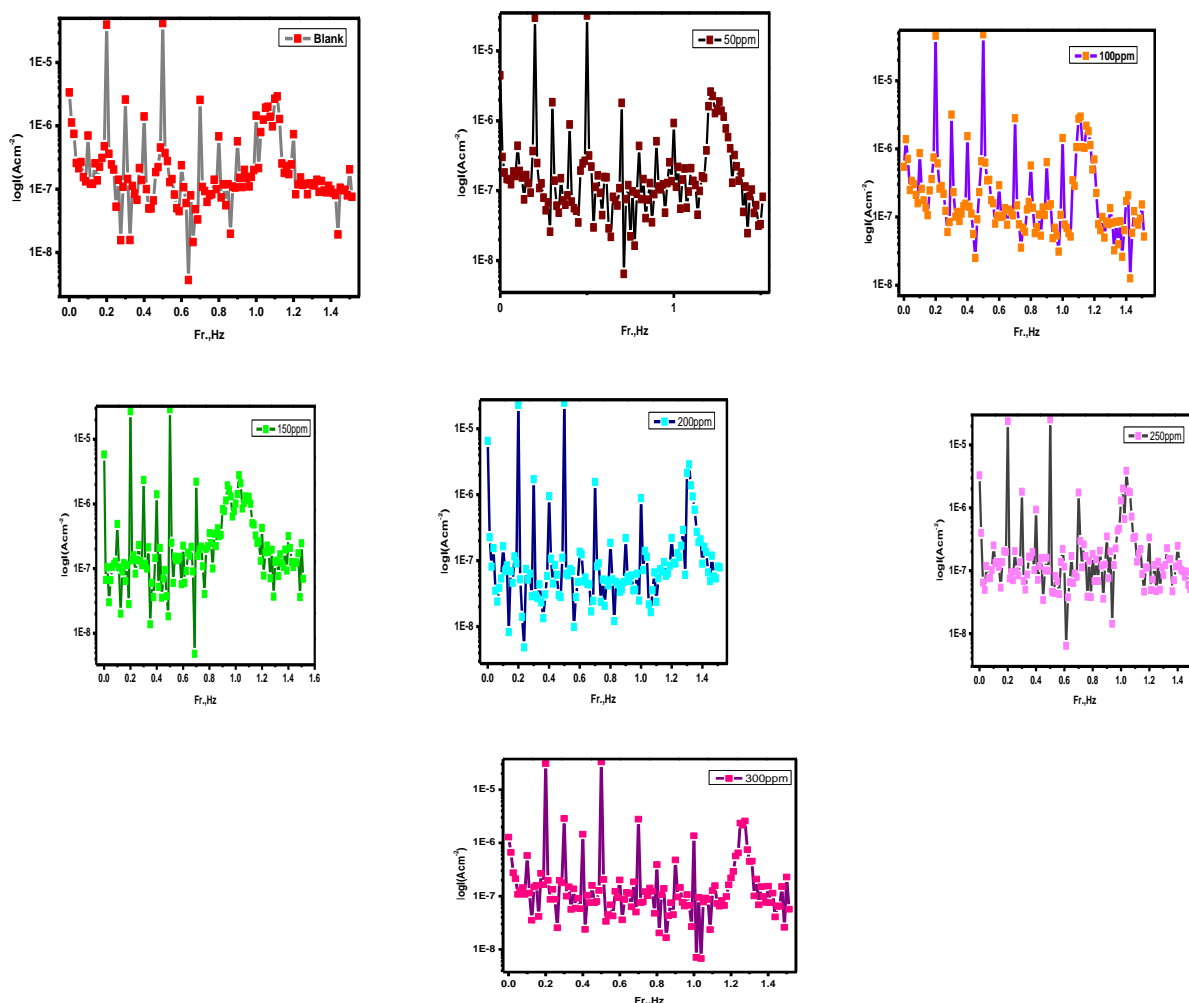


Fig.15. carbon steel intermodulation spectrum at 1 M HCl in the absence and presence of various concentrations from ECS at 25 °C.

### 3.3. The Surface Exams

#### 3.3.1. AFM assessment.

To verify the earlier results, this study used atomic force microscopy, a highly accurate technique (AFM). The resolution for organizing nanoscale fractions during this scan, however, is fixed at 1000 times the optical deviation limitation [133]. Table 8 displays the findings of this check. The symbol Sq, which represents the average measured height deviations obtained inside the assessment length and measured from the mean line, stands for root-mean-square roughness. The sign Sa, which displays the average departure of the roughness prole at all spots throughout the evaluation, from an average line, stands for the average roughness. The letter P-V stands for the peak-to-valley height values that are the highest. Figure 16 displays three illustrations of alloy. The first model

just covers alloy, the second model includes carbon steel that has been exposed to 1 M HCl for three h., and the third model includes alloy that has been exposed to 1 M HCl while also containing the greatest concentration of ECS. Atmospheric corrosion caused a minor flaw on the polished carbon steel surface. Figure 16 shows the corroded alloy surface without the extract of ECS soaked in 1 M HCl. The surface heights of carbon steels Sq, Sa, and P-V are 591.08 nm, 496.932 nm, and 3933 nm, respectively. These findings show that the refined alloy's surface is smoother than the alloy surface that has been immersed in 1 M HCl. While deep in 1 M HCl, the typical surface roughness of the alloy fell from 496.932 to 185.5 nm when 300 ppm of ECS was present. Because the ECS particles adhered to the carbon steel surface and smoothed the surface, the maximum concentration of ECS reduced the contact of the carbon steel with hydrochloric acid. This

stopped the surface of the alloy from corroding uniformly (Fig.16).

**Table 8:** The morphological information of the surface of carbon steel after being immersed for a day in a solution of 1 M HCl without and with 300 ppm of ECS.

Models	$S_q$ (nm)	$S_a$ (nm)	Maximum peak-to-valley height(nm)
Refined alloy	24.793	20.6278	136.067
Alloy in 1 molar hydrochloric acid	591.08	496.932	3933
Alloy+1M HCl+300ppm ECS	203.5	185.5	3856.5

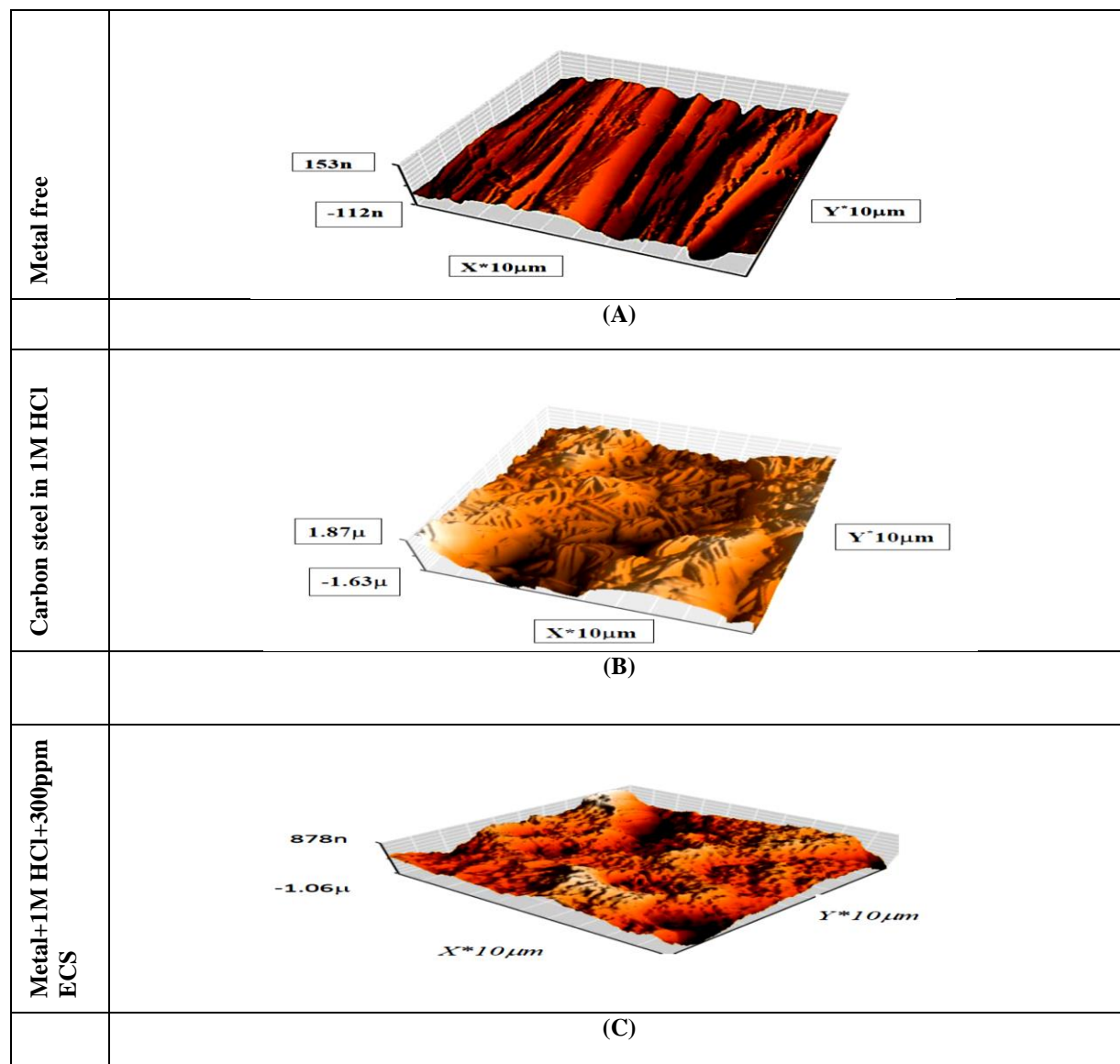


**Fig.16.** (A) free AFM image of a carbon steel electrode surface. (B) the surface of the alloy electrode after one day in a 1 M HCl solution, and (C) the surface of the alloy electrode afterwards one day in a 1 M HCl solution containing 300 ppm ECS.

### 3.3.2. Technique of X-ray photoelectron spectroscopy (XPS)

Noticing how an adsorbed layer forms on the alloy surface in a hydrochloric acid medium using the XPS technique, the type of ECS adsorption was demonstrated. Figure 17 shows the XPS decay spectra of ECS implanted in the surface membrane produced in an inhibitor composition-containing solution are displayed. These spectra are all explained by applying the essential binding energies that have been offered in the literature, according to published research on the

explanation of XPS spectra for thin membranes. As shown in Fig.17(a-f), the carbon steel XPS spectrum recorded at 1M hydrochloric acid in the presence of 300 ppm ECS contains components of Cl 2p, Fe 2p, O 1s, N1s, and C 1s. Table 9 provides the binding energies (BE, eV) for each peak component along with the matching assignment [134-136]. Three distinct peaks including binding energies of about 286.43, 285.12, and 284.52 eV in the alloy C 1s spectra were discovered in 1 M HCl with 300 ppm ECS. O 1s spectra, by binding energies of 530.33, 532.02, and 529.33 (eV), were present on three unlike peaks.

**Table 9.** The binding energies (eV) for the enormous core positions discovered on the surface of alloy after being subjected to an extract made from ECS.

Core line	1 molar Hydrochloric acid	
	BE, ev	Functions
C1s	286.43 285.12 284.52	C=O, C-C,C-H, C-+O
Fe2p	711.94 723.89 719.82 717.87 727.76 712.42	Fe <sub>2</sub> O <sub>3</sub> , Fe <sub>2</sub> p <sub>1/2</sub> of Fe <sup>3+</sup> , FeOOH, Fe <sub>2</sub> O <sub>3</sub> , FeCl <sub>2</sub> , Ferric compounds satellites
Cl2p	198.01 199.58	FeCl <sub>2</sub>
O1s	530.33 532.02 529.33	Metal oxide, Hydroxide, FeO and Fe <sub>2</sub> O <sub>3</sub>
N1s	399.9	NH <sub>2</sub>

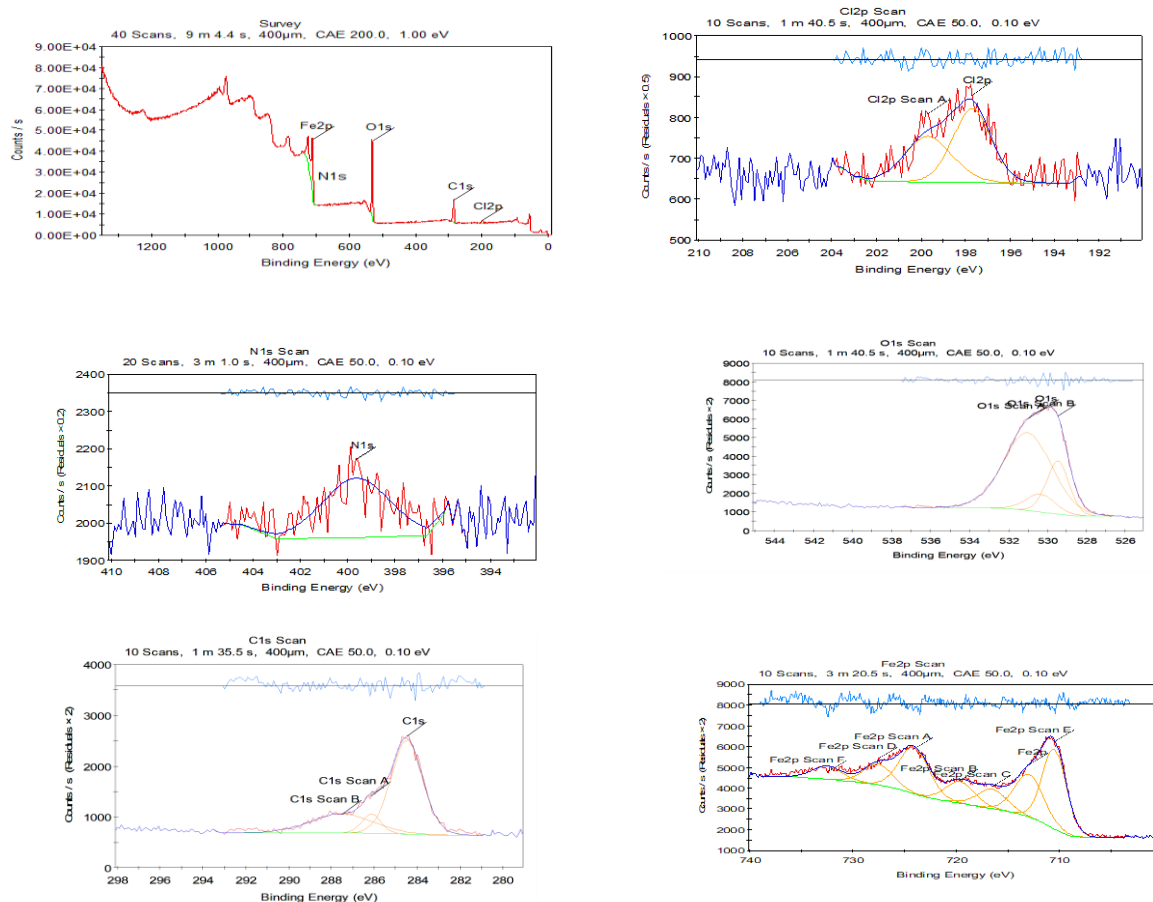


**Fig.17.** Scanning elements, Cl 2p, N1s, O 1s, C 1s, and Fe 2p respectively for photoelectric X-rays for carbon steel at 1 M HCl with 300 ppm ECS.

### 3.3.3. FT-IR evaluation

FT-IR is an effective method for identifying functional groups in various molecules and chemical compounds. In Fig.18, the ECS spectra of a carbon steel coupon are depicted before and after a day of soaking. These graphs demonstrate that before the carbon steel was submerged in 1 M HCl plus 300 ppm ECS, significant peaks were observed at 3383.1, 1646.3, 1435.03, and 725.06  $\text{cm}^{-1}$ , which are comparable to the stretching vibrations of the O-H,

C=O, aliphatic C-H, and Fe, respectively. The infrared spectra obtained after a carbon steel electrode was immersed in the test solution for a day show that all of the functional groups in the ECS under examination are still discernible. These functional groups did not change other than their locations, pointing to a potential interaction between the ECS and the metal surface. As a result, these functional groups can join with  $\text{Fe}^{2+}$  to create complexes that defend the steel against corrosion [137].

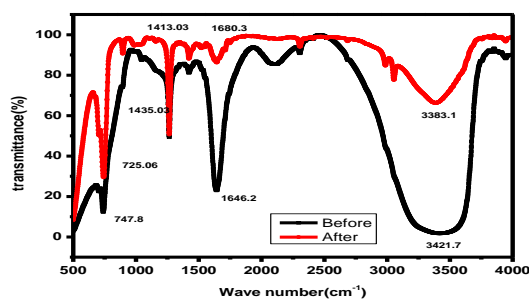


**Fig.18.** FT-IR spectrum of ECS before and after they were adsorbed on a carbon steel surface.

### 3.4. Parameters for quantum chemistry

Like other natural product extracts, the inhibitory activity of ECS can be linked to phytochemical components adhering to the surface of the alloy. It is challenging to accurately experimentally quantify the involvement of several constituents in the overall inhibitory impact due to the biomass extract's complex chemical makeup. To highlight the distinctive contributions of numerous isolated compounds of ECS, the current work used molecular dynamics simulations and quantum chemical parameters. (Fig.20 & Fig.21) depict the two scenarios where the ECS orbitals (LUMO and HOMO orbitals) have the best geometric structure (neutral and protonated). Higher  $E_{\text{HOMO}}$  values show a compound's better capacity to provide electrons to the vacant d-orbital of the metal surface, whereas lower  $E_{\text{LUMO}}$  values show a compound's capacity to accept electrons [138]. The material with the most facilities successfully inhibits corrosion. The data of  $E_{\text{HOMO}}$  and  $E_{\text{LUMO}}$  derived in Table 10 reveal that the investigated ECS can either give or receive electrons. In its neutral state, linoleic acid's HOMO orbital is mostly distributed at the carbon atom, but in its protonated state, it is dispersed at the hydroxyl group and carbonyl group. In both the neutral and protonated cases, the hydroxyl group and carbonyl group are where the LUMO orbital at linoleic acid is most widely dispersed. Oleic acid amid' s HOMO orbital is primarily distributed at the carbon atom in its neutral state, but when it is protonated, it is scattered at amid group. The amid group is where the LUMO orbital at the oleic acid amid' s is most extensively spread in both the neutral and protonated scenarios. The HOMO and LUMO orbitals are distributed into the hydroxy group and carbonyl group in the neutral and protonated situations of cetylic acid and stearic acid. Oleanolic acid's HOMO orbital is distributed on the cyclic hydrocarbon in its neutral form, while its LUMO orbital is spread in the carboxyl group. Nevertheless, in its protonated form, both the HOMO and LUMO orbitals are distributed in the cyclic hydrocarbon. In the 2-hydroxyethyl benzoate compound's neutral form, the LUMO orbital is distributed in the benzene ring, but the LUMO orbital is also distributed in the benzoic acid's oxygen. However, in the compound's protonated form, the HOMO orbital is distributed in the benzene ring and the hydroxyl group and LUMO orbital are distributed throughout almost the entire compound. This refers to the entire 2-hydroxyethyl benzoate molecule being adsorbed. In the neutral form, the HOMO orbital is dispersed around the hydroxyl group and cyclic carbons in the stigma sterol molecule, and the LUMO orbital is scattered around the carbon chain, and in a protonated form, the opposite occurs. Both the HOMO

and LUMO orbitals of  $\beta$ -Sitosterol are distributed around the hydroxyl group and cyclic carbon in the neutral form, and in the protonated form, the HOMO orbital is distributed around the cyclic carbon of the hydroxyl group and the LUMO orbital is distributed around the cyclic carbon and hydroxyl group. The energy gap ( $\Delta E$ ), whose size indicates whether or not molecules are reactive during adsorption on the metal surface, is another critical parameter. An inverse correlation exists between the reaction during adsorption and the value of  $\Delta E$ . Compounds with low energy gap values make good corrosion inhibitors because it takes slight ionization energy to knock an electron out of its outer shell orbital [139]. The components of the ECS have a smaller energy gap ( $\Delta E$ ) in the proton form versus the neutral state (Table 11), which may indicate that the extract reacts to the surface of steel more powerfully in the proton form (Fig.19). Moreover, compared to other components, oleanolic acid's protonated and neutral forms have a smaller energy gap [140]. Smaller energy gaps result in softer molecules than larger ones. Because they can carry electrons to their acceptor quickly, soft molecules react faster than tougher molecules. Using the absolute hardness ( $\eta$ ) and softness ( $\sigma$ ) values, it is possible to determine the make-up, stability, and reactivity of molecules. Only the area of the ECS molecule with the maximum value may become adsorbate for the simplest electron transfer [141]. In the corrosion structure, the alloy turns into a Lewis acid, whilst the molecules of the ECS turn into Lewis bases. Soft-base inhibitors are the most efficient for preventing acid corrosion in bulk metals that take mild acids into account. The dipole moment is the third crucial parameter, which is used to move and rationalize the construction [142, 143]. Superior values take into account the likelihood that stronger connections amongst the ECS molecules and the alloy surface were achieved, resulting in more effective inhibition (higher I. E %) and better adsorption. Because an organic dipole and an exciting alloy surface are electrostatically attracted to one another, the physical adsorption of the organic retarder onto the alloy surface is boosted. Therefore, the adsorption molecules' greater dipole moment is preferred. Indicating that the ECS is physically adsorbed on the steel surface as a proton can be, a measurement of dipole moments revealed that the shape of the dipole torque altered considerably in protons [144]. The larger value of the inhibitor molecule makes it more likely for the inhibitor to adsorb onto the carbon steel interface, changing the thickness of the CdI and creating a flawless isolation film on the carbon steel interface, and oleanolic acid has a large value of dipole moment in the protonated form. Despite this, there isn't any evidence in the literature for a relationship

between it and inhibition efficacy [145]. The ability of the electronic inhibitor on the metal surface is said to increase inhibition efficiency if  $\Delta N$  is less than 3.6[146]. Electronegativity is the property of an electron to bind inhibitors ( $\chi$ ). The value of  $\chi_{inh}$  (electronegativity) increases as the desire to adsorb an electron from an alloy surface becomes higher (A protonated form is more valuable). Because of this

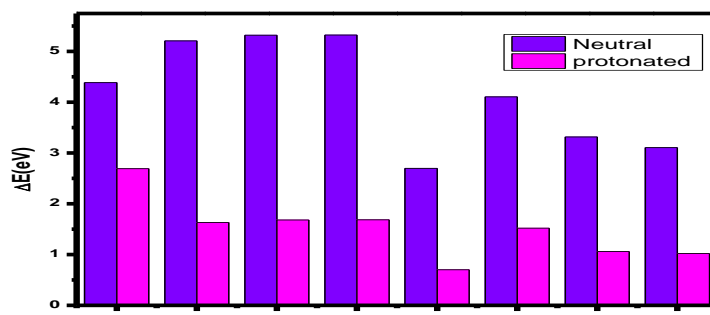
stronger surface interaction between ECS particles with higher electronegativity and the surface of the alloy, inhibition is increased. Compared to earlier research [147], Tables 10 and 11 show that the ECS functions as a powerful inhibitor. Increasing the area of the ECS molecules increases the effectiveness of inhibition because it expands the space where those molecules may interact with the surface of carbon steel.

Table 10 The quantum information for the neutral form of the examined ECS.

Neutral	Linoleic acid	Oleic acid amid	Cetylic acid	Stearic acid
$-E_{HOMO}$ (eV)	-5.374	-5.560	-6.027	-6.025
$-E_{LUMO}$ (eV)	-0.986	-0.355	-0.709	-0.708
$\Delta E$ (eV)	4.384	5.205	5.318	5.320
$\eta$ (eV)	2.192	2.603	2.659	2.660
$\sigma$ (eV) <sup>-1</sup>	0.456	0.384	0.376	0.376
Pi (e.V)	-3.18	-2.957	-3.368	-3.367
$\chi$ (eV)	3.18	2.957	3.368	3.367
dipole moment (debyes)	1.7167	5.3920	2.4783	2.4594
Molecular area (Å <sup>2</sup> )	390.597	405.2656	357.824	397.585
$\Delta N_{max}$ (e)	0.250	0.254	0.171	0.172
Neutral	Oleanolic acid	2-hydroxyethyl benzoate	Stigma sterol	$\beta$ -Sitosterol
$-E_{HOMO}$ (eV)	6.367	6.273	5.623	5.249
$-E_{LUMO}$ (eV)	3.670	2.168	2.489	2.145
$\Delta E$ (eV)	2.697	4.105	3.314	3.104
$\eta$ (eV)	1.35	2.1	1.66	1.55
$\sigma$ (eV) <sup>-1</sup>	0.740	0.467	0.602	0.645
Pi (e.V)	-5.018	-4.221	-4.056	-3.697
$\chi$ (eV)	5.018	4.221	4.056	3.697
dipole moment (debyes)	7.86	4.98	6.83	6.34
Molecular area (Å <sup>2</sup> )	510.3	204.142	430.4	435.9
$\Delta N_{max}$ (e)	-0.273	0.014	0.068	0.188

**Table 11.** The quantum information for the protonated form of the examined ECS.

Protonated	Linoleic acid	Oleic acid amid	Cetylic acid	Stearic acid
-E <sub>HOMO</sub> (eV)	-4.630	-4.916	-5.464	-5.494
-E <sub>LUMO</sub> (eV)	-1.940	-3.285	-3.782	-3.811
ΔE (eV)	2.69	1.631	1.682	1.683
η (eV)	1.345	0.816	0.841	0.841
σ (eV) <sup>-1</sup>	0.745	1.23	1.19	1.19
Pi (e.V)	-3.285	-4.100	-4.623	-4.653
χ (eV)	3.285	4.100	4.623	4.653
dipole moment (debyes)	40.4090	45.1523	45.1589	51.0793
Molecular area (Å <sup>2</sup> )	410.418	410.163	371.0268	410.15
ΔN <sub>max</sub> (e)	0.369	0.11	-0.203	-0.221
Protonated	Oleanolic acid	2-hydroxyethyl benzoate	Stigma sterol	β-Sitosterol
-E <sub>HOMO</sub> (eV)	4.67	4.39	5.38	5.26
-E <sub>LUMO</sub> (eV)	3.97	2.87	4.32	4.24
ΔE (eV)	0.7	1.52	1.06	1.02
η (eV)	0.35	0.76	0.53	0.51
σ (eV) <sup>-1</sup>	2.87	1.32	1.89	1.96
Pi (e.V)	-4.32	-3.63	-4.85	-4.75
χ (eV)	4.32	3.63	4.85	4.75
dipole moment (debyes)	76.9	45.8	56.8	57.6
Molecular area (Å <sup>2</sup> )	546.79	230.5	446.9	463.7
ΔN <sub>max</sub> (e)	-0.057	0.427	-0.538	-0.460

**Fig.19.** ΔE values for several compounds in the extract of ECS



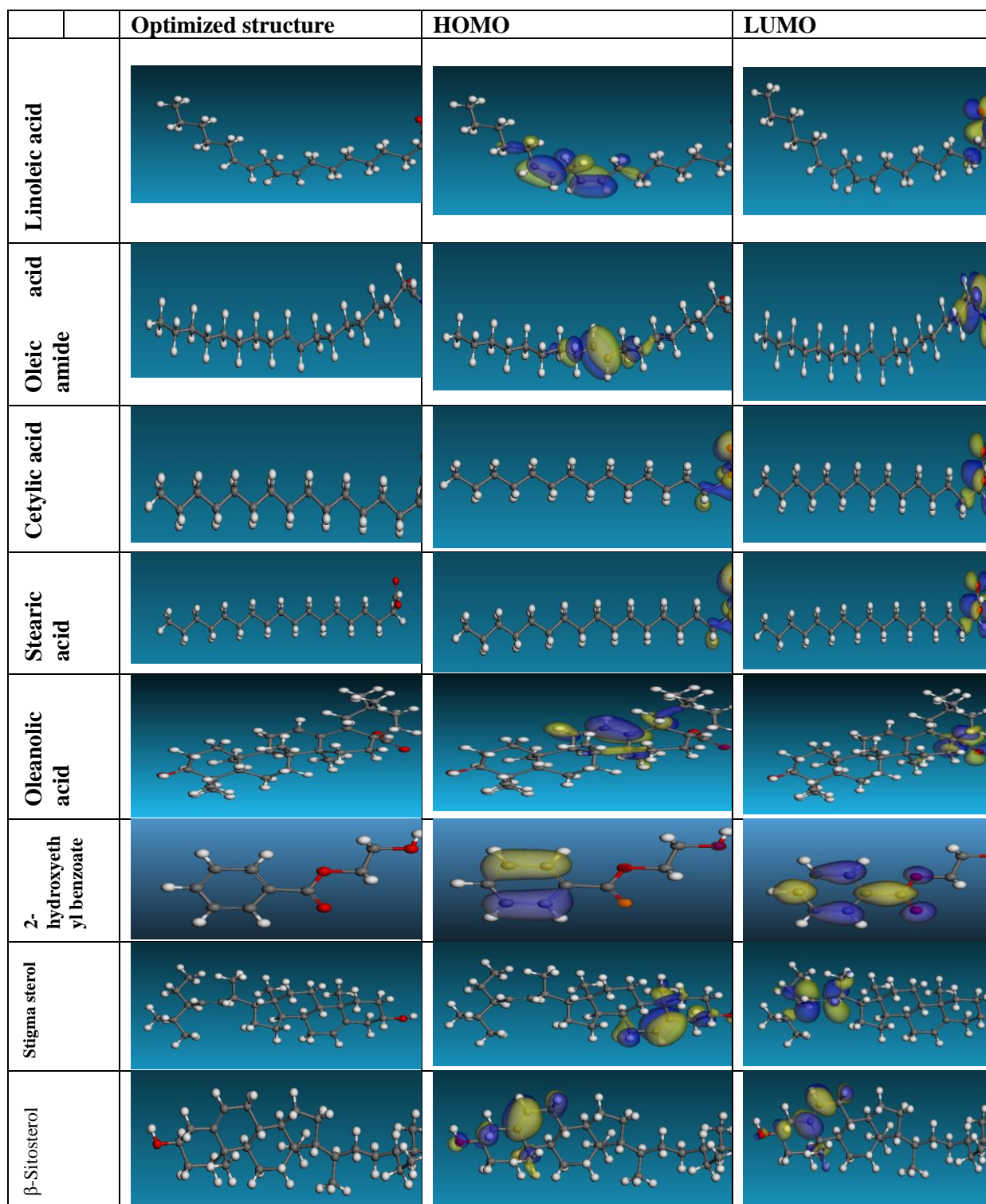


**Fig. 20.** The HOMO and LUMO orbital shapes and molecular structure optimization for vital components in ECS were determined using the Dmol3/GGA/BOP approach (Neutral).

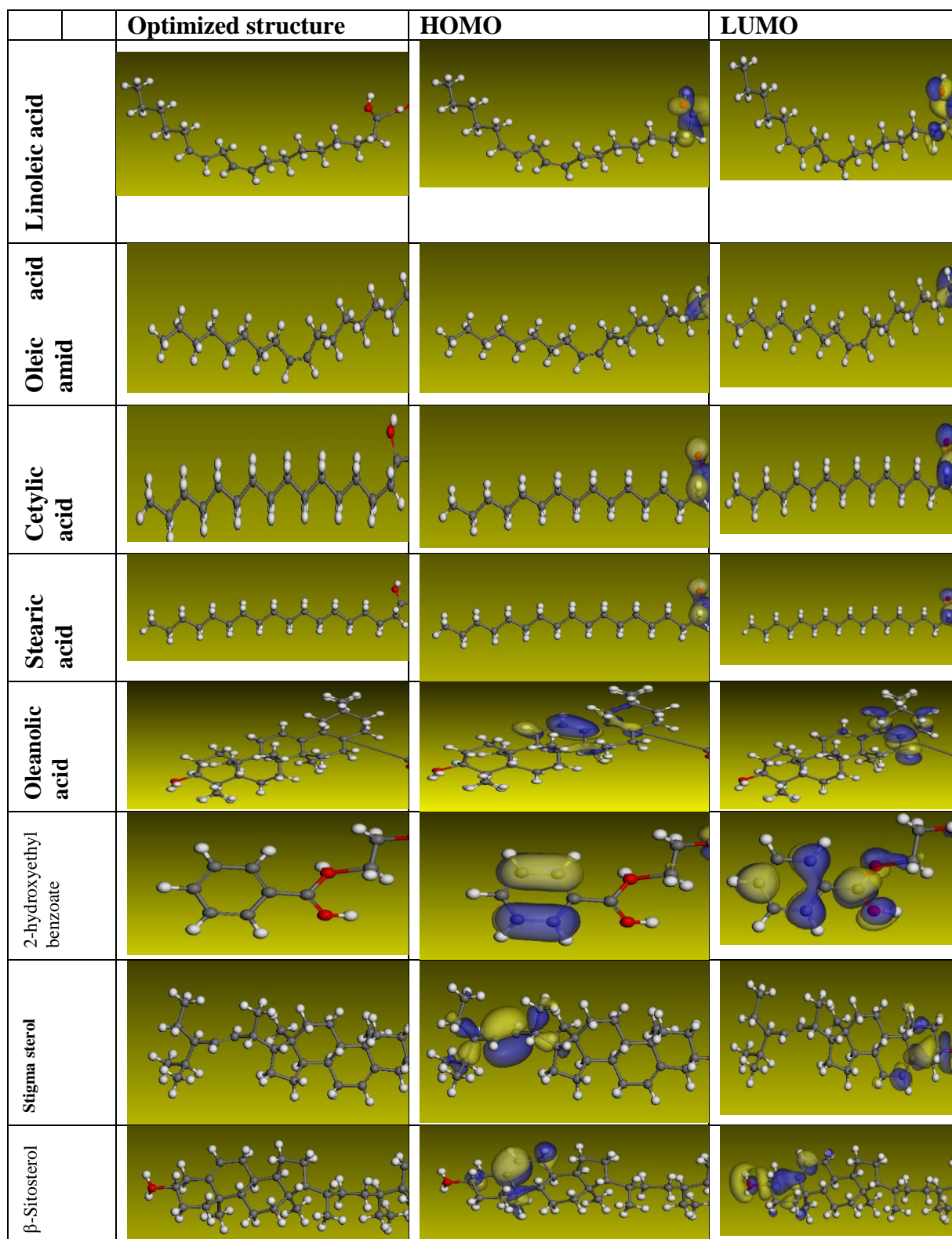


**Fig. 21.** The HOMO and LUMO orbital shapes and molecular structure improvement for vital components in ECS were determined using the Dmol3/GGA/BOP approach (Protonated).

### 3.4.1. Mulliken charges and Fukui indices.

The position of the donor and acceptor of the molecule's active centres will be identified using Mulliken atomic charges and Fukui indices. The Mulliken distribution values are negative and positive, indicating that the donor-acceptor active sites in the ECS compounds enhance these species' allergy to iron atoms. Similar behavior in the duration of total negative charge (TNC) was seen, with the TNC declining as the ECS was protonated, according to the illustration in Fig.22 [148]. The electrostatic attraction between protonated constituents and chloride ions that adsorbed on the surface of the alloy shows an increase in the structural interaction of protonated particles. According to TNC, oleanolic acid has a better ability than other chemicals to function as an attractor. They can therefore attach to metal surfaces more successfully. In settings with acidity (HCl), heteroatom-containing organic compounds can protonate, resulting in the production of positively charged particles. The chloride anions that are widely dispersed on the tissue's surface interact with these molecules. This concept will be applied here to examine the effects of protonation on the local centers

of inhibitory substances. As additional markers (Fukui's index (FI)), Figs. (23), and figs(S19-S25) illustrated the atoms of the molecules under study with higher values of  $f_k^+$  and  $f_k^-$  in both protonated and unprotonated systems. This figure's analysis as a total reveal that each molecule contains unique atoms for both electrophilic and nucleophilic assault systems. The particle in the molecule that has the highest Fukui function ( $f_k^+$ ) is related to the LUMO and increases reactivity to donor reagent, and is the one that is the most frequently attacked by nucleophiles. For electrophilic assault, the atom in the target molecule with the highest values of the HOMO-related Fukui function ( $f_k^-$ ), which also gives reactivity in the direction of an acceptor substance, is chosen. In the protonated state, the values of  $f^-$  for atoms reduced because the donor property was lost because the centres were blocked by protons  $H^+$ , and the values of  $f^+$  for particles grew after protonation since these atoms could take electrons Fig.(23), and Figs. (S19-S25). Also, various particles in the self-same compound own varied  $f^+$  and  $f^-$  values, which means that the extract scan receives and supplies electrons in two separate situations (protonated and neutral systems).

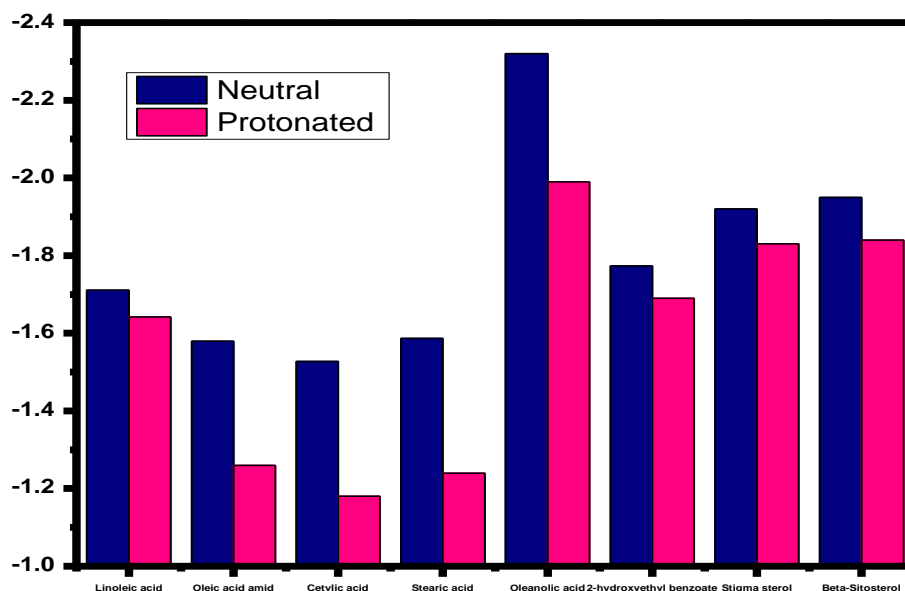


Fig.22. Protonated and unprotonated molecules are extracted from ECS using TNC.

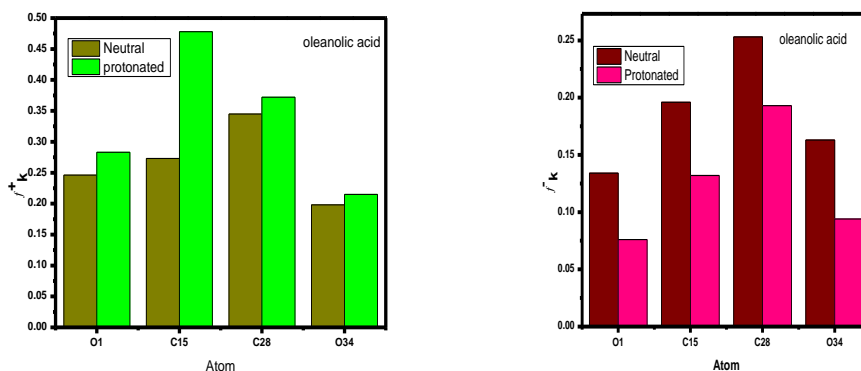
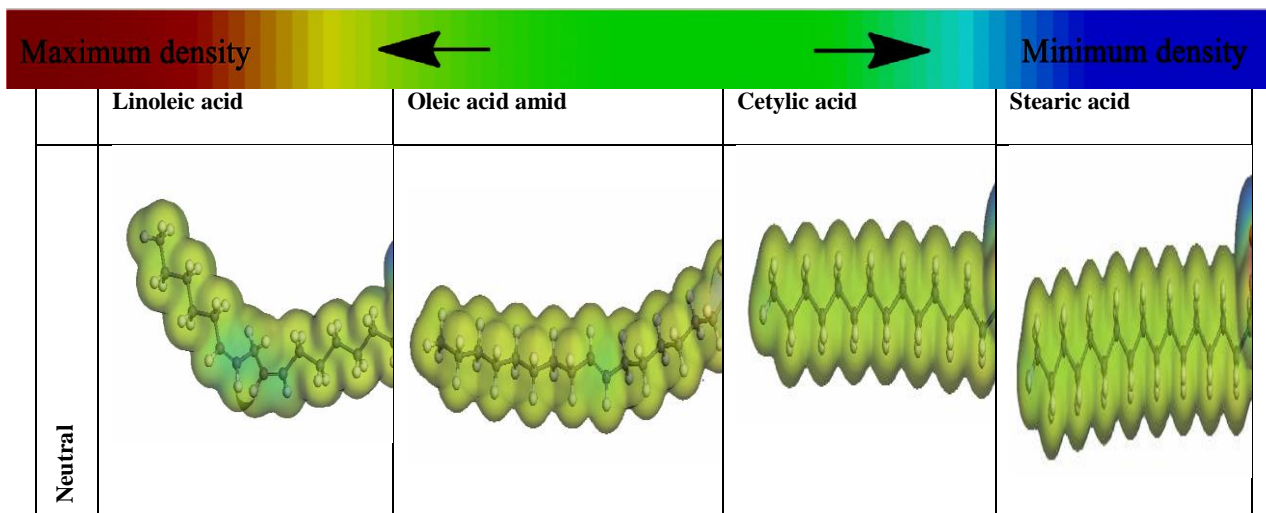


Fig.23. A graphic depiction of oleanolic acid's Fukui indices for its more reactive atoms in both their un-protonated and protonated forms.

### 3.4.2. Molecular electrostatic potential (MESP).

The location of a chemical reaction has long been determined using the molecular electrostatic potential (MESP). The electrostatic potential is colored differently at different locations on the surface of the electron density. The electrically active and electrophilic area depicted in red is in a region with a mainly negative electrostatic potential. Blue parts (the

nucleophilic zone) have the maximum positive electrostatic potential, while green areas (the areas with little possibility) are shown by the color green[149,150]. The majority of heteroatoms and double conjugate bonds can be found in places with a high electron density. Indicating negative zones that encourage electrophilic attacks are oxygen and nitrogen groups. According to Fig. 24, blue hydrogen atoms are more likely to be attacked by nucleophiles.



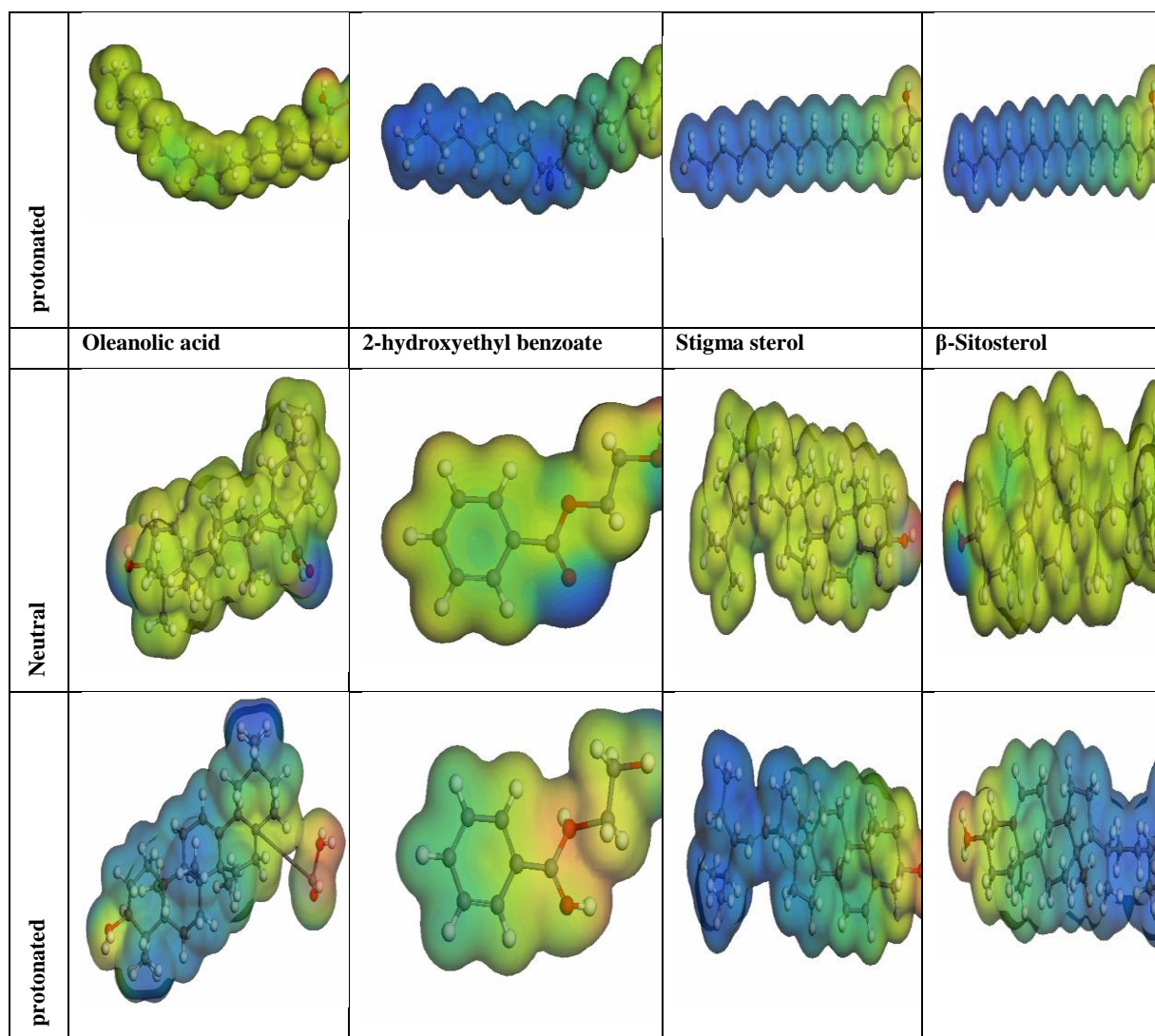


Fig. 24. The electrostatic potentials of the protonated and un-protonated molecules as the contour of the inhibitor's electrostatic field.

### 3.5. Monte Carlo experiments

For the adsorption of ECS (adsorbate) on the Fe (110) crystal, the adsorption locator module was selected as the ideal structure (adsorbent) in the corrosion-simulating fluid (250 H<sub>2</sub>O molecules plus 10 H<sub>3</sub>O<sup>+</sup> and 10 Cl<sup>-</sup>). In the maximum and sideways perspectives of the iron (110) substrate, respectively, Fig. 25 and Fig. 26 depict the adsorption mechanisms of the ECS molecules in neutral and protonated forms. The results of the Monte Carlo simulation for the total energy, solid adsorption, and deformation energies are presented in Table 12. Total energy (kcal mol<sup>-1</sup>) computation for the substrate and ECS as a result of combining molecular energies from solid adsorption with deformation energies.  $dE_{ads}/dNi$  is a unit of measurement for the energy obtained during the separation of one of the adsorbate particles from the adsorbent substrate (kcal mol<sup>-1</sup>). The ECS adsorption

energies are displayed in Table 12. Therefore, as shown by theoretical and practical research, it is likely that the molecules of the ECS are adsorbed on the surface of carbon steel, producing adsorbed coatings and protecting the surface from corrosion caused by hydrochloric acid solution. The studied components worked effectively in solution, as shown by Tables 12 and 13 and earlier investigations [34,148] (high adsorption energy). A careful examination reveals that the molecular structure of the local molecule is parallel to the surface [151]. The components of the retarding particle will take on this adsorption pattern to increase the contact area or surface covering capabilities with the alloy. Instead of causing unwanted chloride anion assaults, the increased metal/inhibitor contact zone will reduce substrate access [140,141]. When a charged proton component is present, it is predicted that the electron transfer from the metallic surface to the elements of the ECS takes place in reverse,

reversing the reaction. ECS molecules strongly adsorb on the alloy surface to form sturdy adsorbent layers that shield the alloy surface from hydrochloric solution acid corrosion, as shown in theoretical and practical research (Table 13). We studied the adsorption of molecules in a vacuum and an acidic (neutral and proton) environment (Figs. 25–27). In the existence of an aqueous solution, the adsorption energies increase above the vacuum value, demonstrating that ECS molecules adsorption on the alloy surface is more efficient (Tables 12 and 143 for further details). The

following formulas can be used to determine the amount of energy that ECS will adsorb onto the Fe (110) contact [140].

$$E_{binding} = -E_{interact} \quad (22)$$

$$E_{interact} = E_{tot} - (E_{sub} + E_{inh}) \quad (23)$$

$E_{tot}$  stands for the system's overall energy in the simulation. Water molecules and substrate energy are denoted by the symbol  $E_{subs}$  respectively.

**Table 12.** The data and settings used to simulate Monte Carlo to adsorb iron -ECS(neutral)

Factors(Neutral)	Oleic acid amide	Linoleic acid	Cetylic acid	Stearic acid
Total energy(kcal /mol)	-4957.262	-5041.256	-4973.196	-4989.064
Adsorption energy(kcal /mol)	-4869.39	-4946.619	-4869.514	-4879.29
Rigid adsorption energy(kcal /mol)	-5044.3	-5128.38	-5042.73	-5054.164
Deformation energy(kcal /mol)	174.9	181.76	173.21	174.87
dE <sub>ad</sub> /dNi (kcal /mol)	-80.26	-135.56	-51.84	-76.08
Factors(protonated)	Oleanolic acid	2-hydroxyethyl benzoate	Stigma sterol	β-Sitosterol
Total energy(kcal /mol)	-4896.050	-4871.797	-5078.714	-4935.789
Adsorption energy(kcal /mol)	-4953.077	-4900.031	-5005.435	-4859.818
Rigid adsorption energy(kcal /mol)	-5031.353	-5073.618	-5189.961	-5036.609
Deformation energy(kcal /mol)	78.28	173.59	184.526	176.79
dE <sub>ad</sub> /dNi (kcal /mol)	-158.739	-113.530	-213.082	-33.289

**Table 13.** The data and settings used to simulate Monte Carlo to adsorb iron -ECS (protonated)

Factors(protonated)	Oleic acid amide	Linoleic acid	Cetylic acid	Stearic acid
Total energy(kcal /mol)	-5024.999	-5045.8313	-5035.209	-5006.409
Adsorption energy(kcal /mol)	-4970.224	-4987.666	-4963.814	-4928.950
Rigid adsorption energy(kcal /mol)	-5149.731	-5164.262	179.32684421	-5106.277
Deformation energy(kcal /mol)	179.5	176.595	179.33	177.33
dE <sub>ad</sub> /dNi (kcal /mol)	-145.36	-196.27	-176.55	-123.43
Factors(protonated)	Oleanolic acid	2-hydroxyethyl benzoate	Stigma sterol	β-Sitosterol
Total energy(kcal /mol)	-5105.382	-4940.502	-5210.708	-5010.9183
Adsorption energy(kcal /mol)	-11930.44	-4939.728	-5210.708	-4941.450
Rigid adsorption energy(kcal /mol)	-5206.185	-5116.179	-5328.867	-5121.971
Deformation energy(kcal /mol)	-6724.252	176.451	184.81	180.521
dE <sub>ad</sub> /dNi (kcal /mol)	-1.97	-61.990	-171.944	-150.33

**Table 14.** shows the data and settings used to simulate Monte Carlo to adsorb iron -ECS (vacuum)

<b>Factors</b>	<b>Oleic acid amide</b>	<b>Linoleic acid</b>	<b>Cetylic acid</b>	<b>Stearic acid</b>
<b>Total energy(kcal /mol)</b>	-274.91	-238.58	-241.39	-266.226
<b>Adsorption energy(kcal /mol)</b>	-187.04	-180.40	-169.99	-188.768
<b>Rigid adsorption energy(kcal /mol)</b>	-192.197	-189.27	-174.072	-193.08
<b>Deformation energy(kcal /mol)</b>	5.158	8.87	4.085	4.316
<b>dE<sub>ad</sub>/dNi (kcal /mol)</b>	-187.039	-180.40	-169.99	-188.767
<b>Factors</b>	<b>Oleanolic acid</b>	<b>2-hydroxyethyl benzoate</b>	<b>Stigma sterol</b>	<b>β-Sitosterol</b>
<b>Total energy(kcal /mol)</b>	-84.872	-67.650	-261.454	-263.377
<b>Adsorption energy(kcal /mol)</b>	-147.042	-95.878	-194.80	-193.90
<b>Rigid adsorption energy(kcal /mol)</b>	-56.987	-96.6996	-210.20	-207.62
<b>Deformation energy(kcal /mol)</b>	-90.055	0.8212	15.40	13.715
<b>dE<sub>ad</sub>/dNi (kcal /mol)</b>	-147.043	-95.87	-194.80	-193.90

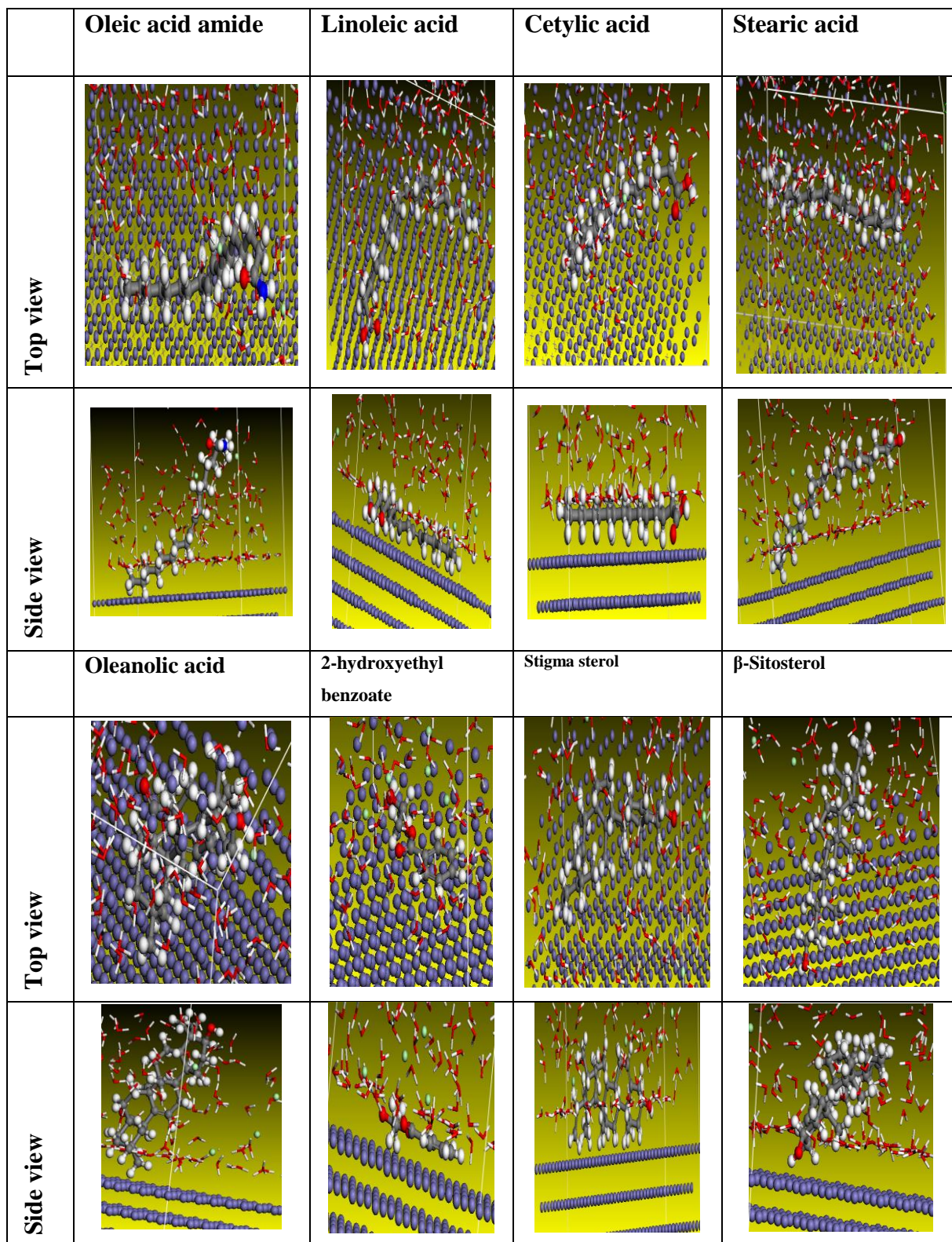


Fig.25. The adsorption locator module's recommendation for the best formation for the adsorption of ECS on carbon steel (110) (neutral form).



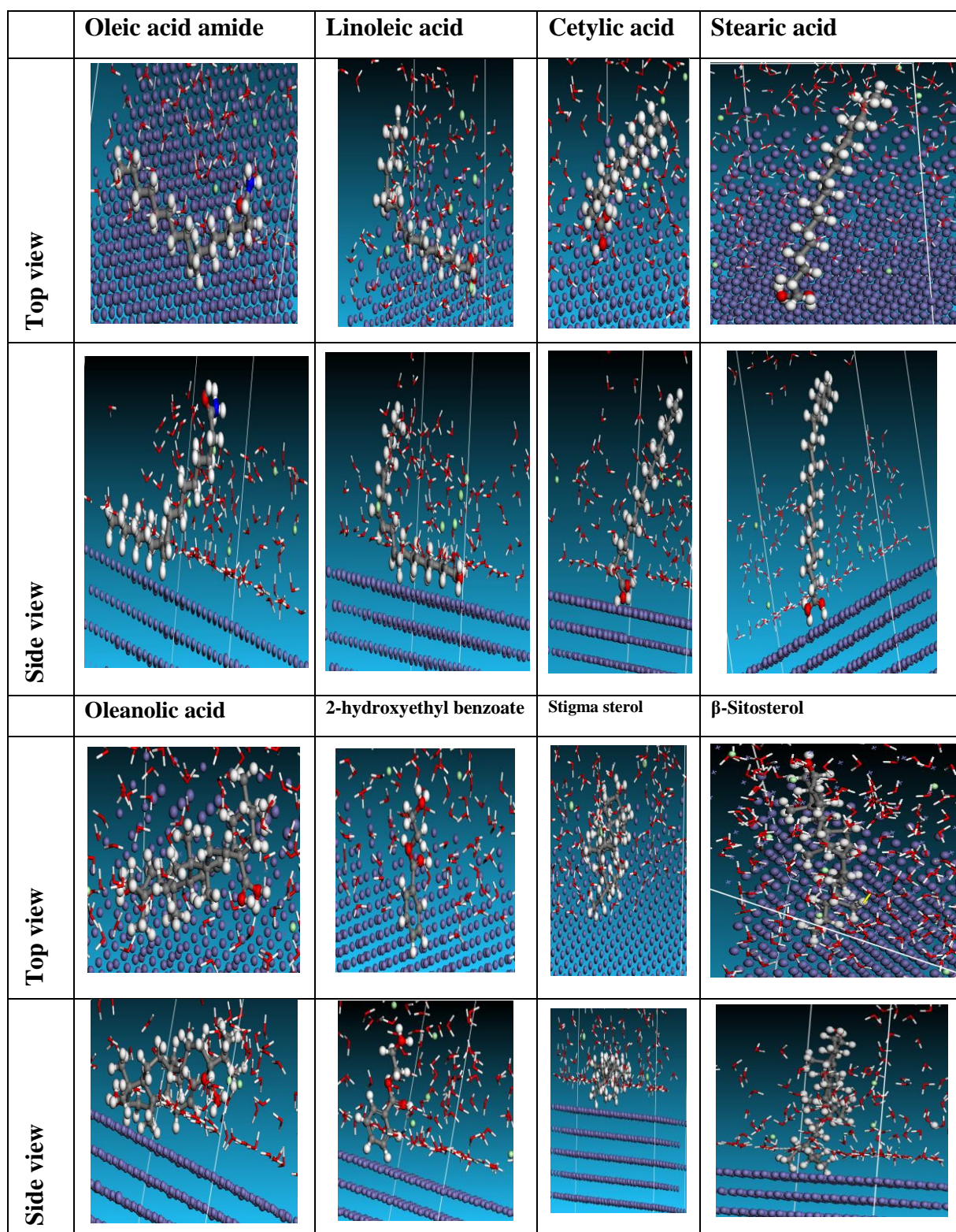


Fig.26. The adsorption locator module's recommendation for the best formation for the adsorption of ECS on carbon steel (110) (protonated form).

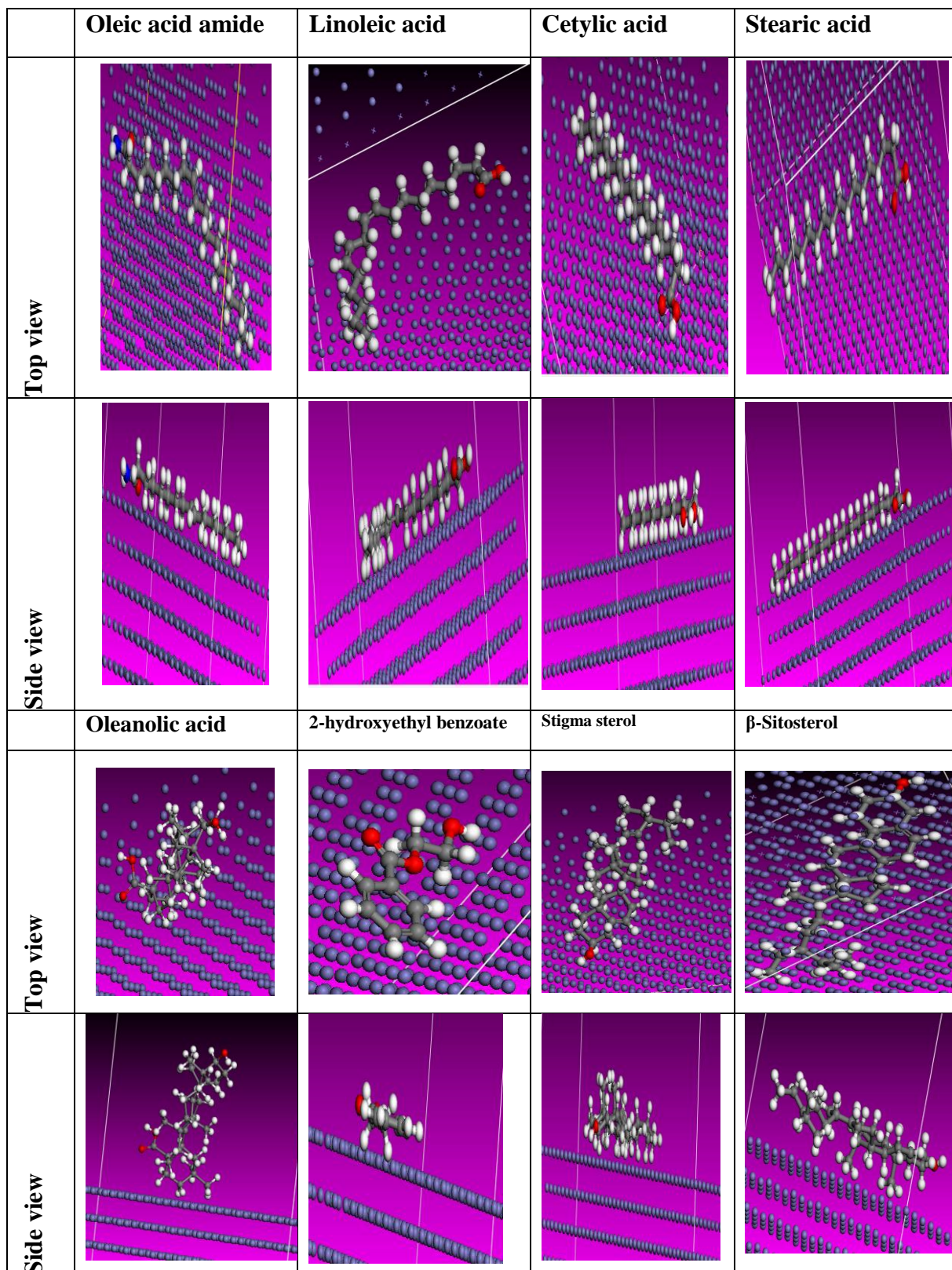
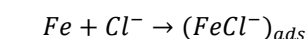


Fig. 27. The adsorption locator module's recommendation for the best formation for the adsorption of ECS on carbon steel (110) (vacuum form).

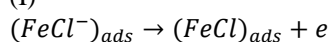
#### 4. Mechanism for inhibiting corrosion

A film that protects the alloy's surface from the corrosive medium was formed by the adsorption of ECS on the alloy surface and was confirmed using theoretical investigations, weight loss, potentiodynamic polarization, EIS, EFM, and numerous surface analysis systems. How much inhibition and interaction the ECS molecules have with the alloy surface depends on the chemical composition, molecular size, and other relevant factors like the reactivity of benzene ring substituents, functional groups, electron density, alloy charge, and the nature of the corrosive middle of the alloy. The reactivity of ECS molecules can be influenced by two different types of functional groups. Since the benzene ring has electron-withdrawing groups, the cyclic  $\pi$ -system's electron density is decreased as a result of the removal of electrons (making the ring electron deficient and less reactive), they were identified as the disruptive groups, carbonyl groups and carboxylic acid. Binding aromatic rings, in contrast, electron-donating groups like the hydroxyl group on the one hand, stabilize an electron by giving electrons to the reaction position, which is the ring that is more reactive and rich in electrons [152]. The main ways that the ECS molecule reacts with the surface of an alloy, according to the literature, are adsorption mechanisms like chemical and/or physical adsorption [153,154]. The progression of alloy corrosion in hydrochloric acid has been anticipated to occur in several phases [153,154].

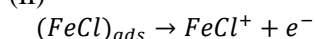
Anodic site reactions:



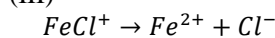
(I)



(II)

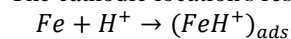


(III)

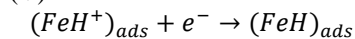


(IV)

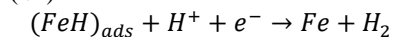
The cathodic location's responses



(V)



(VI)



(VII)

The procedure described above shows that the degree of corrosion of iron in hydrochloric acid is measured by Fe anodic decay and cathodic hydrogen growth. The inhibitory mechanism of hetero atom adsorption on the alloy surface in the current investigation can be explained by one or more of the

following hypotheses. There are two ways that the molecules of the ECS can adsorb on the surface of iron: first, by transferring the unshared pair electrons from oxygen, nitrogen atoms or/and  $\pi$  electron charge to the iron's unoccupied d-orbital, which takes place in the anodic region and has low energy; second, by forming a coordinate chemical bond between the molecules of the ECS and the surface of the iron. As a result of electrostatic attraction (physical adsorption) brought on by the protonation of the ECS molecules by chloride anions, bridges amid the ECS molecules and alloy are created utilizing  $(FeCl^-)_{ads}$ . The ECS is then adsorbed on the cathodic region to vie with ions of hydrogen (equation V), causing an increase in the cathode polarization [153]. The use of chemical and electrical interactions is another possibility [154]. The second approach is supported by considerable experimental results and theoretical computations. Hydrochloric acid protonates the ECS molecules right away and then transforms them into positively charged inhibitor species. Zero charge potential known as the carbon steel surface charge at zero, must be determined (ZCP). It applies the formula ( $E_{corr} - E_q = 0$ ). A positive surface charge is present when ( $E_{corr} - E_q = 0$ ) is greater than zero [145]. Iron's ZCP in HCl solution is, as earlier established [146],  $E_q = -530$  mV vs SCE. When comparing ECS components to SCE, the maximum  $E_{corr}$  values are  $-467$  mV at 300 ppm (refer to Table 5). Consequently, it is projected that Fe-ZCP will have a value of 63 mV, which indicates a positively charged alloy surface. It is anticipated that the positively charged steel surface and the protonated charged ECS will repel one another electrostatically. Hydrochloric acid with negatively charged chloride ions ( $Cl^-$ ) should be applied to the surface of the alloy due to the electrostatic attraction amongst the anionic species and the protonated species of ECS on the electrolyte/alloy interface. When ECS molecules with positive charges adhere to the surface of the alloy, the chloride bridge helps to give the first coating of adsorption. This method involves the physical adsorption of these molecules, which results in a thin layer of protection covering the entire alloy surface and a significant decrease in the speed of corrosion of carbon steel. The second discovery is that the molecules of ECS have a predicted value of  $\Delta G^0_{ads}$  that is fewer than 20 kJ/ mol. (Table 4), representing an electrostatic relationship between the charged ECS particles and the negatively charged iron surface, or physisorption. As said by the XPS findings, a complex film of molecules made up of iron oxide/hydroxide and an extract of ECS form on the metal surface. By separating the corrosive media in hydrochloric acid, these components have a shield that prevents the corrosion of carbon steel.

## 5. Conclusion

Utilising weight loss, electrochemical methods, and surface analysis, experimental studies of the corrosion inhibition of ECS as an efficient green inhibitor on carbon steel in 1M HCl solution were conducted. A correlation between weight loss and electrochemical studies (EIS, EFM, and potentiodynamic) showed that inhibitory efficacy rises with increasing ECS concentration, peaking at 300 ppm. ECS is a mixed type inhibitor. The outcomes showed that the presence of the ECS inhibitor identified by FT-IR, AFM, and XPS spectra may conform to the complex film generated between the carbon steel and the active groups found in the ECS. The reactive sites of the ECS components with corrosion inhibition abilities have a strong tendency to adsorb on the carbon steel surface, according to theoretical studies that also included molecular dynamics and quantum mechanics simulations. All the results also showed significant correlations between them. As a consequence of combining theoretical calculations with experimental findings, it can be said that the ECS has the potential to be created as an environmentally benign inhibitor for carbon steel corrosion.

## 6. Participation

All participants in the manuscript are mentioned as they participated in the manuscript in equal:

1-Prof. H.S. Gadaw

2- Prof. Marzough A Albalawi

## Declaration of interests

The authors declare that they have no known competing financial interests or personal relationships that could have appeared to influence the work reported in this paper.

## 7. Funding

No funding for this research

## 8. References

- [1] H. Bourazmi, M. Tabyaoui, L. El Hattabi, Y. El Aoufir, M. Taleb Methanolic Extract of *Salvia Officinalis* plant as a green inhibitor for the corrosion of carbon steel in 1 M HCl, *J. Mater. Environ. Sci.*, 9 (2018) 928-938, [10.26872/jmes.2018.9.3.103](https://doi.org/10.26872/jmes.2018.9.3.103)
- [2] M.A. Hegazy, A.S. El-Tabei, A.H. Bedair, M.A. Sadeq, An investigation of three novel nonionic surfactants as corrosion inhibitor for carbon steel in 0.5 M H<sub>2</sub>SO<sub>4</sub> *Corros. Sci.*, 54 (2012) 219-230, [10.1016/J.CORSCI.2011.09.019](https://doi.org/10.1016/J.CORSCI.2011.09.019)
- [3] H.I. Husnu Gereng, *Schinopsis lorentzii* extract as a green corrosion inhibitor for low carbon steel in 1 M HCl solution *Rech. En Chim. Ind. Tech.* (2012) 780-787, [10.1021/ie201776q](https://doi.org/10.1021/ie201776q)
- [4] F.E.T. Heakal, A.E. Elkholy, Gemini surfactants as corrosion inhibitors for carbon steel *J. Mol. Liq.*, 230 (2017) 395-407, [10.1016/J.MOLLIQ.2017.01.047](https://doi.org/10.1016/J.MOLLIQ.2017.01.047)
- [5] F.A. Ayeni, S. Alawode, D. Joseph, P. Sukop, V. Olawuyi, T.E. Alonge, O.O. Alabi, O. Oluwabunmi, F.I. Alo, Investigation of *Sida acuta* (wire weed) plant extract as corrosion inhibitor for aluminium-copper-magnesium alloy in acidic medium, *J. Miner. Mater. Charact. Eng.*, 2(2014)286-291  
<http://dx.doi.org/10.4236/jmmce.2014.24033>
- [6] S. Bilgiç, Plant extracts as corrosion inhibitors for mild steel in HCl media - review I *Int. J. Corros. Scale Inhib.*, 10 (2021), pp. 145-175, [10.17675/2305-6894-2021-10-1-9](https://doi.org/10.17675/2305-6894-2021-10-1-9)
- [7] S. Zehra, Mohammad Mobin, Jeenat Aslam, An overview of the corrosion chemistry, *3(2022)23* <https://doi.org/10.1016/B978-0-323-85405-4.00012-4>
- [8] C. Verma, Corrosion: basics and adverse effects, basics and adverse effects. *Elsevier EBooks*, (2022)1-10, <https://doi.org/10.1016/B978-0-323-90589-3.00020-3>
- [9] E. Machnikova, K.H. Whitmire, N. Hackerman Corrosion inhibition of carbon steel in hydrochloric acid by furan derivatives *Electrochim. Acta.*, 53 (2008) 6024-6032, [10.1016/J.ELECTACTA.2008.03.021](https://doi.org/10.1016/J.ELECTACTA.2008.03.021)
- [10] A. Bousskri, A. Anejjar, M. Messali, R. Salghi, O. Benali, Y. Karzazi, S. Jodeh, M. Zougagh, E.E. Ebenso, B. Hammouti Corrosion inhibition of carbon steel in aggressive acidic media with 1-(2-(4-chlorophenyl)-2-oxoethyl)pyridazinium bromide, *J. Mol. Liq.*, 211 (2015) 1000-1008, [10.1016/J.MOLLIQ.2015.08.038](https://doi.org/10.1016/J.MOLLIQ.2015.08.038)
- [11] Q. Hu, Y. Qiu, G. Zhang, X. Guo, Capsella bursa-pastoris extract as an eco-friendly inhibitor on the corrosion of Q235 carbon steels in 1 mol•L<sup>-1</sup> hydrochloric acid, *Chin. J. Chem. Eng.*, 23 (2015) 1408-1415, [10.1016/J.CJCHE.2015.05.002](https://doi.org/10.1016/J.CJCHE.2015.05.002)
- [12] K. Stanly Jacob, G. Parameswaran, Corrosion inhibition of mild steel in hydrochloric acid solution by Schiff base furoin thiosemicarbazone, *Corros. Sci.*, 52 (2010) 224-228, [10.1016/J.CORSCI.2009.09.007](https://doi.org/10.1016/J.CORSCI.2009.09.007)
- [13] P. Lowmunkhong, D. Ungtharak, P. Sutthivaiyakit, Tryptamine as a corrosion inhibitor of mild steel in hydrochloric acid solution, *Corros. Sci.*, 52 (2010) 30-36, [10.1016/J.CORSCI.2009.08.039](https://doi.org/10.1016/J.CORSCI.2009.08.039)

- [14] B. Tan, S. Zhang, X. Cao, A. Fu, L. Guo, R. Marzouki, W. Li, Insight into the anti-corrosion performance of two food flavors as eco-friendly and ultra-high performance inhibitors for copper in sulfuric acid medium, *Journal of Colloid and Interface Science*, 609 (2022) 838–851. <https://doi.org/10.1016/j.jcis.2021.11.085>
- [15] B. Tan, W. Lan, S. Zhang, H. Deng, Y. Qiang, A. Fu, Y. Ran, J. Xiong, R. Marzouki, W. Li, Passiflora edulia Sims leaves Extract as renewable and degradable inhibitor for copper in sulfuric acid solution, *Colloids and Surfaces A: Physicochemical and Engineering Aspects* 645 (2022) 128892, <https://doi.org/10.1016/j.colsurfa.2022.128892>
- [16] Y. Feng, J. He, Y. Zhan, J. An, B. Tan, Insight into the anti-corrosion mechanism Veratrum root extract as a green corrosion inhibitor, *J. Mol. Liq.* 334 (2021), 116110.
- [17] A. Berrissoul, E. Loukili, N. Mechbal, F. Benhiba, A. Guenbour, B. Dikici, A. Zarrouk, A. Dafali, Anticorrosion effect of a green sustainable inhibitor on mild steel in hydrochloric acid, *J. Colloid Interface Sci.* 580 (2020) 740–752.
- [18] A.R. Shahmoradi, M. Ranjbarhane, A.A. Javidparvar, L. Guo, E. Berdimurodov, B. Ramezanzadeh, Theoretical and surface/electrochemical investigations of walnut fruit green husk extract as effective inhibitor for mild-steel corrosion in 1M HCl electrolyte, *J. Mol. Liq.* 338 (2021), 116550.
- [19] J. Zhang, L. Zhang, G. Tao, A novel and high-efficiency inhibitor of 5-(4-methoxyphenyl)-3h-1,2-dithiole-3-thione for copper corrosion inhibition in sulfuric acid at different temperatures, *J. Mol. Liq.* 272 (2018) 369–379.
- [20] Z.S. Aziz, R.A. Majed, M.H. Abd, S. A. Naser, Corrosion Inhibition of Carbon Steel in Seawater Solution by Wild Clary Extracts, *AIP Conference Proceedings* 2475, 040016 (2023); <https://doi.org/10.1063/5.0104435>
- [21] M. Alimohammadi, M. Ghaderi, A. Ramazani S.A., M. Mahdavian, Falcaria vulgaris leaves extract as an eco-friendly corrosion inhibitor for mild steel in hydrochloric acid media, *Scientific Reports* 13 (2023) 3737 <https://doi.org/10.1038/s41598-023-30571-6>
- [22] R. Ihamdane, M. Tiskar, B. Outemsaa, L. Zelmat, O. Dagdag, A. Berisha, E. Berdimurodov, E. E. Ebenso, A. Chaouch, Essential Oil of Origanum vulgare as a Green Corrosion Inhibitor for Carbon Steel in Acidic Medium, *Arabian Journal for Science and Engineering*, <https://doi.org/10.1007/s13369-023-07693-0>
- [23] A.Y. El-Etre, Natural honey as corrosion inhibitor for metals and alloys. I. copper in neutral aqueous solution, *Corros. Sci.*, 40 (1998), 1845–1850, [10.1016/S0010-938X\(98\)00082-1](https://doi.org/10.1016/S0010-938X(98)00082-1)
- [24] K.O. Orubite, N.C. Oforika, Inhibition of the corrosion of mild steel in hydrochloric acid solutions by the extracts of leaves of Nypa fruticans Wurmb Mater. Lett., 58 (2004), 1768–1772, [10.1016/J.MATLET.2003.11.030](https://doi.org/10.1016/J.MATLET.2003.11.030)
- [25] G.O. Avwiri, F.O. Igho, Inhibitive action of Vernonia amygdalina on the corrosion of aluminium alloys in acidic media, *Mater. Lett.*, 57 (2003), 3705–3711, [10.1016/S0167-577X\(03\)00167-8](https://doi.org/10.1016/S0167-577X(03)00167-8)
- [26] A. Dehghani, G. Bahlakeh, B. Ramezanzadeh, M. Ramezanzadeh, Potential role of a novel green eco-friendly inhibitor in corrosion inhibition of mild steel in HCl solution: detailed macro/micro-scale experimental and computational explorations, *Constr. Build. Mater.*, 245 (2020), 118464, [10.1016/J.CONBUILDMAT.2020.118464](https://doi.org/10.1016/J.CONBUILDMAT.2020.118464)
- [27] A. Y. El-Etre, “Inhibition of acid corrosion of carbon steel using aqueous extract of olive leaves,” *Journal of Colloid and Interface Science*, vol. 314, no. 2, pp. 578–583, 2007.
- [28] P. B. Raja and M. G. Sethuraman, “Natural products as corrosion inhibitor for metals in corrosive media—A review,” *Materials Letters*, vol. 62, no. 1, pp. 113–116, 2008.
- [29] A. M. Abdel-Gaber, B. A. Abd-El-Nabey, and M. Saadawy, “The role of acid anion on the inhibition of the acidic corrosion of steel by lupine extract,” *Corrosion Science*, vol. 51, no. 5, pp. 1038–1042, 2009.
- [30] P. Bothi Raja and M. G. Sethuraman, “Solanum tuberosum as an inhibitor of mild steel corrosion in acid media,” *Iranian Journal of Chemistry and Chemical Engineering*, vol. 28, no. 1, pp. 77–84, 2009.
- [31] Fdil R, Tourabi M, Derhali S, et al. Evaluation of alkaloids extract of Retama monosperma (L.) Boiss. stems as a green corrosion inhibitor for carbon steel in pickling acidic medium by means of gravimetric, AC impedance and surface studies. *JMES*. 2018;9(1):358–369.
- [32] El-Etre AY. Inhibition of acid corrosion of carbon steel using aqueous extract of olive leaves. *J Colloid Interface Sci.* 2007;314(2):578–583.
- [33] H. S. Gadow, M. Fakeeh, Green inhibitor of carbon steel corrosion in 1 M hydrochloric acid: Eruca sativa seed extract (experimental and theoretical studies), *RSC Adv.*, 12(2022) 8953–8986.
- [34] Ramezanzadeh M, Bahlakeh G, Ramezanzadeh B, et al. Adsorption mechanism and synergistic corrosion-inhibiting effect between the green Nettle leaves extract and Zn<sup>2+</sup> cations on carbon steel. *J Ind Eng Chem.* 2019;77:323–343.

- [35] H. Gadow, M.M.Motawea, Investigation of the corrosion inhibition of carbon steel in hydrochloric acid solution by using ginger roots extract, *RSC Adv.* 7 (2017)24576–24588, <https://doi.org/10.1039/C6RA28636D>
- [36] H. S. Gadow and A. S. Fouda, Black Tea as Green Corrosion Inhibitor for Carbon Steel in 1 M Hydrochloric Acid Solutions, *International Journal of Advanced Research* 2(2014) 233-243
- [37] H. S. Gadow, M. M. Motawea and H. M. Elabbasy, Investigation of myrrh extract as a new corrosion inhibitor for a-brass in 3.5% NaCl solution polluted by 16 ppm sulfide, *RSC Adv.*, 7(2017) 29883–29898, [DOI:10.1039/c7ra04271j](https://doi.org/10.1039/c7ra04271j).
- [38] A. S. Fouda, H. S. Gadow, E. G. Abd Elal and M. I. El- Tantawy, Corrosion Inhibition of Aluminium by Rice Straw Extract in 2 M Hydrochloric Acid Solution, *J. Bio-Tribo-Corros.*,7( 2021) 102–118, [DOI: 10.1007/s40735-021-00527-2](https://doi.org/10.1007/s40735-021-00527-2).
- [39] A. S. Fouda, E. E El-shereafy, A. A. Hathoot and N. M Elbahrawi, Corrosion Inhibition of Al by Cerium rubrum Extraction Hydrochloric Acid Environment, *J. Bio- Tribo- Corros.*, 2020, 6, 37–53, [DOI: 10.1007/s40735-020-0330-9](https://doi.org/10.1007/s40735-020-0330-9).
- [40] M. A. M. El-Haddad, A. B. Radwan, M. H. Sliem, W. M. I. Hassan and A. M. Abdullah, Highly efficient ecofriendly corrosion inhibitor for mild steel in 5M HCl at elevated temperatures: experimental & molecular dynamics study, 9(2019) 3695–3709, [DOI: 10.1038/s41598-019-40149-w](https://doi.org/10.1038/s41598-019-40149-w).
- [41] F. Bouhlal, N. Labjar, F. Abdoun, A. Mazkour, M. Serghini-Idrissi, M. El Mahi, E. M. Lotfy and S. El Hajjaji, *Int. J. Corros.*, 2020(2020)4045802–4045815, [DOI: 10.1155/2020/4045802](https://doi.org/10.1155/2020/4045802).
- [42] E. A. S, ahin, R. Solmaz, I. H. Gecibesler and G. Kardas, Adsorption ability, stability and corrosion inhibition mechanism of phoenix dactylifera extract on mild steel, *Mater. Res. Express*, 7(2020) 016585–01658594, [DOI:10.1088/2053-1591/ab6ad3](https://doi.org/10.1088/2053-1591/ab6ad3).
- [43] A. Diab, S. M. Abd El-Haleema, Corrosion Inhibition of Copper in Acidic Solution by using a Natural Product as Henna Extract (*Lawsonia inermis* L), *Egypt. J. Chem.* 65( 2)(2022) 103 – 111, [DOI: 10.21608/EJCHEM.2021.66539.3747](https://doi.org/10.21608/EJCHEM.2021.66539.3747)
- [44] S. Marzorati, L. Verotta and S. P. Trasatti, Green Corrosion Inhibitors from Natural Sources and Biomass Wastes, *Molecules*, 24(2019) 48–71, [DOI: 10.3390/molecules24010048](https://doi.org/10.3390/molecules24010048).
- [45] O. O. Fadare, A. E. Okoronkwo and E. F. Olasehinde, Assessment of anti-corrosion potentials of extract of *Ficus asperifolia*-Miq (Moraceae) on mild steel in acidic medium, *Afr. J. Pure Appl. Chem.*, 10(1)(2016) 8–22. <http://dx.doi.org/10.5897/AJPAC2015.0651>.
- [46] M. Manickam, D. Sivakumar, B.Thirumalairaj, and M. Jaganathan, Corrosion Inhibition of Mild Steel in 1 mol L<sup>-1</sup> HCl Using Gum Exudates of *Azadirachta indica*, *Hindawi Publishing Corporation Advances in Physical Chemistry* 2016 ( 2016) 5987528-5987540 <http://dx.doi.org/10.1155/2016/5987528>
- [47] A. Z. Hassana, M. K.G. Mekhaela, A. G. Hanna, A. Simonb, Phytochemical investigation of *Corchorus olitorius* and *Corchorus capsularis* (Family Tiliaceae) that grow in Egypt, *Egyptian Pharmaceutical Journal*, 18 ( 2) (2019). DOI: 10.4103/epj.epj\_51\_18
- [48] M. Gobara, B.Zaghloul, A.Baraka, M. Elsayed, M. Zorainy, M.Mokhtar Kotb , H. Elnabarawy, Green corrosion inhibition of mild steel to aqueous sulfuric acid by the extract of *Corchorus olitorius* stems, *Mater. Res. Express* 4 (2017) 046504, <https://doi.org/10.1088/2053-1591/aa664a>
- [49] K.Marušić, H.Otmačić Ćurković, Croat., Self-Assembling Monolayers of Stearic Acid in Protection of Steel *Chem. Acta*91(4) 427–433, DOI: 10.5562/cca3436
- [50] ASTM, ASTM G 31-72, Standard Recommended Practice for the Laboratory Immersion Corrosion Testing of Metals, American Society for Testing and Materials, Philadelphia, PA, USA,1990.
- [51] A.S. Fouda, E.E El-Shereafy, A.A.Hathoot, N.M.El-bahrawi , Corrosion inhibition of al by cerium rubrum extraction hydrochloric acid environment. *J Bio-Tribo-Corr* (2020)6–37. <https://doi.org/10.1007/s40735-020-0330-9>
- [52] T.Attar, A. Benchadli, B.Messaoudi, N. Benhadria, E. Choukchou-Braham, Experimental and Theoretical Studies of Eosin Y Dye as Corrosion Inhibitors for Carbon Steel in Perchloric Acid Solution. *Bulletin of Chemical Reaction Engineering & Catalysis*, 15 (2)(2020)454-464 [doi:10.9767/bcrec.15.2.7753.454-464](https://doi.org/10.9767/bcrec.15.2.7753.454-464)
- [53] L.EMEMBOLU, C. IGWEGBE, Investigation of Temperature Correlations on Corrosion Inhibition of Carbon Steel in Acid Media by Flower Extract, *European J. Eng. App. Sci.* 5(1)(2022)29-36, DOI: 10.55581/ejeas.1127813
- [54] K.Khaled , Evaluation of electrochemical frequency modulation as a new technique for monitoring corrosion and corrosion inhibition of carbon steel in perchloric acid using hydrazinecarbodithioic acid derivatives. *J Appl Electrochem* 39(2009)429–438. <https://doi.org/10.1007/s10800-008-9688-y>
- [55] SO.Adejo, SG .Yiase, L.Leke, M.Onuche, M.V. Atondo, T.T.Uzah, Corrosion studies of mild steel

- in the sulphuric acid medium by the acidimetric method. *Int J Corros Scale Inhib*, 8(1)(2019) 50–61.  
<https://doi.org/10.17675/2305-6894-2019-8-1-5>.
- [56] L. Zhou, Y. L. Lv, Y. X. Hu, J. H. Zhao, X. Xia and X. Li, Experimental and theoretical investigations of 1,3,5 tris(4-aminophenoxy)benzene as an effective corrosion inhibitor for mild steel in 1 M HCl, *J. Mol. Liq.*, 249(2018) 179–187, DOI: [10.1016/j.molliq.2017.10.129](https://doi.org/10.1016/j.molliq.2017.10.129).
- [57] H. M. Abd El-Lateef, M. A. Abo-Riya and A. H. Tantawy, Empirical and quantum chemical studies on the corrosion inhibition performance of some novel synthesized cationic Gemini surfactants on carbon steel pipelines in acid pickling processes, *Corros. Sci.*, 108(2016) 94–110, DOI: [10.1016/j.corsci.2016.03.004](https://doi.org/10.1016/j.corsci.2016.03.004).
- [58] R. G. Pearson, Absolute electronegativity and hardness: application to inorganic chemistry, *Inorg. Chem.*, 1988, 27, 734–740, DOI: [10.1021/ic00277a030](https://doi.org/10.1021/ic00277a030). 73 A. Kokalj, On the HSAB based estimate of charge transfer between adsorbates and metal surfaces, *Chem. Phys.*, 393(2012) 1–12, DOI: [10.1016/j.chemphys.2011.10.021](https://doi.org/10.1016/j.chemphys.2011.10.021).
- [59] N. Kovačević and A. Kokalj, DFT Study of Interaction of Azoles with Cu(111) and Al (111) Surfaces: Role of Azole Nitrogen Atoms and Dipole–Dipole Interactions, *J. Phys. Chem. C*, 115(49)(2011) 24189–24197, DOI: [10.1021/jp207076w](https://doi.org/10.1021/jp207076w).
- [60] A. Toghan, H. S. Gadow, H. M. Dardeer and H. M. Elabbasy, New promising halogenated cyclic imides derivatives as potential corrosion inhibitors for carbon steel in hydrochloric acid solution, *J. Mol. Liq.*, 325(2021) 115136–115156, DOI: [10.1016/j.molliq.2020.115136](https://doi.org/10.1016/j.molliq.2020.115136).
- [61] H. M. Elabbasy and H. S. Gadow, Study the effect of expired tenoxicam on the inhibition of carbon steel corrosion in a solution of hydrochloric acid, *J. Mol. Liq.*, 321(2021) 114918–114935, DOI: [10.1016/j.molliq.2020.114918](https://doi.org/10.1016/j.molliq.2020.114918).
- [62] Z. Gong, Sh. Peng, X. Huang and L. Gao, Investigation the corrosion inhibition effect of Itraconazole on copper in H<sub>2</sub>SO<sub>4</sub> at different temperatures: combining experimental and theoretical studies, *Materials*, 11(2018) 2107–2123, DOI: [10.3390/ma11112107](https://doi.org/10.3390/ma11112107).
- [63] K. Chkirate, K. Azgaou, H. Elmsellem, B. El Ibrahimy, N.K. Sebbar, E.H. Anouar, M. Benmes saoud, S. El Hajjaji, E.M. Essassi, Corrosion inhibition potential of 2-[(5-methylpyrazol-3-yl)methyl]benzimidazole against carbon steel corrosion in 1 M HCl solution: combining experimental and theoretical studies. *J. Mol. Liq.*, 321 (2021), Article 114750, [10.1016/J.MOLLIQ.2020.114750](https://doi.org/10.1016/J.MOLLIQ.2020.114750)
- [64] A.M. Al-Turkustani, S.T. Arab, R.H. Al-Dahiri, Effect of temperature on the performance of aloe extract and azadirachta indica extract in absence and presence of iodide ions on aluminum corrosion in hydrochloric acid. *J. Mater. Environ. Sci.*, 3 (2012) 1163-1176
- [65] P. Roy, P. Karfa, U. Adhikari, D. Sukul Corrosion inhibition of mild steel in acidic medium by polyacrylamide grafted Guar gum with various grafting percentage: Effect of intramolecular synergism, *Corros. Sci.*, 88 (2014) 246-253, [10.1016/J.CORSCI.2014.07.039](https://doi.org/10.1016/J.CORSCI.2014.07.039)
- [66] D. Brondel, R. Edwards, A. Hayman, D. Hill, S. Mehta, T. Semerad, Corrosion in the oil industry, *Oilfield Rev.* 6 (1994) 4–18.
- [67] D.G. Hill, A. Jones, An engineered approach to corrosion control during matrix acidizing of HTHP sour carbonate reservoir, *Corrosion* (2003). Paper No.03121.
- [68] M.L. Walker, Method and Composition for Acidizing Subterranean Formations, in: US Patent 5,366,643, Halliburton Company, Duncan, Okla, 1994
- [69] M. Pour-Ghaz, O.B. Isgor, P. Ghods, The effect of temperature on the corrosion of steel in concrete. Part 1: simulated polarization resistance tests and model development *Corros. Sci.*, 51 (2009) 415–425, [10.1016/J.CORSCI.2008.10.034](https://doi.org/10.1016/J.CORSCI.2008.10.034)
- [70] H. Lgaz, S.K. Saha, A. Chaouiki, K.S. Bhat, R. S alghi, P. Banerjee Shubhalaxmi, I.H. Ali, M.I. Khan, I.M. Chung Exploring the potential role of pyrazoline derivatives in corrosion inhibition of mild steel in hydrochloric acid solution: Insights from experimental and computational studies, *Build. Mater.*, 233 (2020) 117320, [10.1016/J.CONBUILDMAT.2019.117320](https://doi.org/10.1016/J.CONBUILDMAT.2019.117320)
- [71] R. Hsissou, S. Abbout, A. Berisha, M. Berradi, M. Assouag, N. Hajjaji, A. Elharfi, Experimental, DFT and molecular dynamics simulation on the inhibition performance of the DGDCBA epoxy polymer against the corrosion of the E24 carbon steel in 1.0 M HCl solution, *J. Mol. Struct.*, 1182 (2019) 340–351, [10.1016/J.MOLSTRUC.2018.12.030](https://doi.org/10.1016/J.MOLSTRUC.2018.12.030)
- [72] A. Thomas, M. Prajila, K.M. Shainy, A. Joseph, A green approach to corrosion inhibition of mild steel in hydrochloric acid using fruit rind extract of *Garcinia indica* (Binda), *J. Mol. Liq.*, 312 (2020), Article 113369, [10.1016/J.MOLLIQ.2020.113369](https://doi.org/10.1016/J.MOLLIQ.2020.113369)

- [73] E. Sezer, B. Ustamehmetoglu, Z. Altuntas ~ , Bayır, Kerim , oban, and A.Kalkan, Corrosion Inhibition Effect of 4-(2-Diethylamino-Ethylsulfonyl)-Phthalonitrile and 4,5-Bis(Hexylsulfonyl)-Phthalonitrile
- [74] I. N. Putilova, S. A. Balezin and V. P. Barannik, *Metallic Corrosion Inhibitors*, Pergamon Press, New York, 1960, p. 31-85.
- [75] M. Zunita , D.Wahyuningrum, Buchari, B. Bundjali, Investigation of Corrosion Inhibition Activity of 3-butyl-2,4,5- triphenylimidazole and 3-butyl-2-(2-butoxyphenyl)-4,5-diphenylimidazole toward Carbon Steel in 1% NaCl Solution, *Int. J. Electrochem. Sci.*, 7 (2012) 3274 – 3288, *International Journal of Electrochemistry*, 2011(2011)235360-235365 doi:10.4061/2011/235360
- [76] Siaka A. Abdulfatai, Owa. O Sunday, M. K. Gafar, and J O. Okunola, Corrosion, inhibition efficiency, adsorption behavior, Kinetics and thermodynamic studies of lannea acida ethanol leaves leaves extract on mild steel in hydrochloric acid, 5 (2) (2021) 621-634 doi.:10.33003/fjs-2021-0502-678
- [77] Y. Ziat, N. Abbas, M.Hammi and S. Echihi: An experimental evaluation of inhibiting corrosion effect of phosphate glass on mild steel in acidic solution, *Materials Research Express*, 6(8)2019. <https://doi.org/10.1088/2053-1591/ab1a4b>
- [78] L.TANG, Effect of NaBr on the corrosion of cold rolled steel in 1.0 M phosphoric acid, *J MATER SCI 4 1 (2 0 0 6 ) 1 9 9 1 – 1 9 9 7*.
- [79] X. Li and L. Tang, *Mater. Chem. Phys.*, 2005, 90, 286.
- [80] K. J. Laidler, *Reaction kinetics*, 1st edn, Pergamon Press, New York, 1963, vol. 1.
- 92 J. R. Macdonald and W. B. Johanson, in *Theory in Impedance Spectroscopy*, ed. J. R. Macdonald, John Wiley & Sons, New York, 1987.
- [81] A. Ostovari, S. M. Hoseinieh, M. Peikari, S. R. Shadizadehband S. J. Hashemi, *Corros. Sci.*, 2009, 51(9), 1935–1949.
- [82] C. Lai, B. Xie, L. Zou, X. Zheng, X. Ma and S. Zhu, *Results Phys.*, 7(2017) 3434–3443.
- [83] A. Mohammadi, S. M. A. Hosseini, M. J. Bahrami and M. Shahidi, *Prog. Color, Color. Coat.*, 9(2)(2016) 117–134.
- [84] N. Harckerman and R. M. Hurd, *1st International Congress on Metallic Corrosion*, Butterworths, London, 1962, vol. 166.
- [85] A. S. Fouda, H. E. Megahed, N. Fouad and N. M. Elbahrawi, *J Bio Tribo. Corros.* 2(2016) 16 DOI 10.1007/s40735-016-0046-z
- [86] A.S. Fouda, S.A. Abd El-Maksoud, E.H. El-Sayed, H.A. Elbaz, and A.S. Abousalem, Experimental and surface morphological studies of corrosion inhibition on carbon steel in HCl solution using some new hydrazide derivatives, *RSC Adv.* 11(22)(2021) 13497–13512. doi: 10.1039/d1ra01405f
- [87] A.K. Satapathy, G. Gunasekaran, S.C. Sahoo, K. Amit, P.V. Rodrigues, Corrosion inhibition by Justicia gendarussa plant extract in hydrochloric acid solution, *Corros. Sci.* 51 (12) (2009) 2848–2856, doi:10.1016/j.corsci.2009.08.016.
- [88] S.K. Shukla, M.A. Quraishi, Ceftriaxone: A novel corrosion inhibitor for mild steel in hydrochloric acid, *J. Appl. Electrochem.* 39 (9) (2009) 1517–1523, doi:10.1007/s10800-009-9834-1.
- [89] M.A. Deyab, Corrosion inhibition of heat exchanger tubing material (titanium) in MSF desalination plants in acid cleaning solution using aromatic nitro compounds, *Desalination.* 439 (2018) 73–79, doi:10.1016/j.desal.2018.04.005.
- [90] B.Tan, J. He, S. Zhang, C.Xu, S. Chen, H. Liu, W.Li, Insight into anti-corrosion nature of Betel leaves water extracts as the novel and eco-friendly inhibitors, *Journal of Colloid and Interface Science* 585(2021)287-301, doi:10.1016/j.jcis.2020.11.059
- [91] M. Rizvi, H. Gerengi, S. Kaya, I. Uygur, M. Yıldız, I. Sarioglu, Z. Cingiz, M. Mielniczek and B. El Ibrahimy, Sodium nitrite as a corrosion inhibitor of copper in simulated cooling water, *Sci. Rep.*, 2021, 11, 8353–8368, doi:10.1038/s41598-021-87858-9.
- [92] R. H. B. Beda, P. M. Niamien, E. B. Avo Bil' e and A. Trokourey, Inhibition of Aluminium Corrosion in 1.0 M HCl by Caffeine: Experimental and DFT Studies, *Adv. Chem.*, 2017(2017) 6975248–6975257, doi: 10.1155/2017/6975248.
- [93] Q. H. Dinh, T. Duong and N. P. Cam, A Study of 1-Benzyl-3-phenyl-2-thiourea as an Effective Steel Corrosion Inhibitor in 1.0 M HCl Solution, *J. Chem.*, 2021, 2021, 5519411–5519424, doi: 10.1155/2021/5519411.
- [94] A. A. Al-Amiery, A. H. Kadhum, A. H. M. Alobaidy, A. B. Mohamad and P. S. Hoon, Novel Corrosion Inhibitor for Mild Steel in HCl, *Materials*, 2014, 7(2), 662–672, doi:10.3390/ma7020662.
- [95] J. M. Thomas and W. J. Thomas, *Introduction to the Principles of Heterogeneous Catalysis*, 5th edn, Academic Press, London, 1981, p. 14.
- [96] M.A. Migahed, M. Abd-El-Raouf, A.M. Al-Sabagh, H.M. Abd-El-Bary, Effectiveness of some nonionic surfactants as corrosion inhibitors for carbon steel pipelines in oil fields, *Electrochim. Acta* 50 (2005) 4683–4689, <https://doi.org/10.1016/j.electacta.2005.02.021>.



- [97] G. Moretti, F. Guidi, F. Fabris, Corrosion inhibition of mild steel in 0.5M HCl by 2-butyl hexahydropyrrolo [1,2-b][1,2]oxazole, *Corros. Sci.* 76 (2013) 206–218, <https://doi.org/10.1016/j.corsci.2013.06.044>.
- [98] A.M. Elsharif, S.A. Abubshait, I. Abdulazez, H.A. Abubshait, Synthesis of a new class of corrosion inhibitors derived from natural fatty acid: 13-Docosenoic acid amide derivatives for oil and gas industry, *Arab. J. Chem.* 13 (2020) 5363–5376, <https://doi.org/10.1016/j.arabjc.2020.03.015>.
- [99] Q. Yan, G. Ma, W. Wang, Study of the corrosion of stainless steel with fatty acid/paraffin/graphite composite phase change materials, *Journal of Physics*, 2076 (2021) 012037. doi:10.1088/1742-6596/2076/1/012037
- [100] X. Liu, S. Chen, H. Ma, G. Liu, L. Shen, Protection of iron corrosion by stearic acid and stearic imidazoline self-assembled monolayers, *Applied Surface Science* 253 (2006) 814–820. doi:10.1016/j.apsusc.2006.01.038
- [101] R. Fuchs-Godec, A Synergistic Effect between Stearic Acid and (+)- $\alpha$ -Tocopherol as a Green Inhibitor on Ferritic Stainless Steel Corrosion Inhibition in 3.0% NaCl Solution, *Coatings*, 11(2021) 971. <https://doi.org/10.3390/coatings11080971>
- [102] I.A. Hermoso-Diaz, A.E. Foroosan, J.P. Flores-De los Rios, L.L. Landeros-Martinez, J. Porcayo-Calderon, J.G. Gonzalez-Rodriguez, Electrochemical and quantum chemical assessment of linoleic acid as a corrosion inhibitor for carbon steel in sulfuric acid solution, *Journal of Molecular Structure* 1197 (2019) 535e546. <https://doi.org/10.1016/j.molstruc.2019.07.085>.
- [103] M. Prbakaran, S.-Hyun Kim, A. Sasireka, V. Hemapriya, Ill-Min Chung,  $\beta$ -Sitosterol isolated from rice hulls as an efficient corrosion inhibitor for mild steel in acidic environments, *New J. Chem.*, 41(2017) 3900-3907. DOI: 10.1039/c6nj03760g.
- [104] D. Bajpai Tripathy, M. Murmub, P. Banerjee, M. Ahmad Quraishid, Palmitic acid based environmentally benign corrosion inhibiting formulation useful during acid cleansing process in MSF desalination plants, *Desalination* 472 (2019) 114128, <https://doi.org/10.1016/j.desal.2019.114128>
- [105] M. Yadav, U. Sharma and P. Yadav, Corrosion inhibitive properties of some new isatin derivatives on corrosion of N80 steel in 15% HCl, *Int. J. Ind. Chem.*, 4(2013) 6.
- [106] L. Zhou, Y.-L. Lv, Y.-X. Hu, J.-H. Zhao, X. Xia, X. Li, Experimental and theoretical investigation of 1,3,5-tris (4-aminophenoxy) benzene as an effective corrosion inhibitor for mild steel in 1 M HCl, *J. Mol. Liq.* 249 (2018) 179–187, <https://doi.org/10.1016/j.molliq.2017.10.129>.
- [107] A. Zaher, A. Chaouiki, R. Salghi, A. Boukhraz, B. Bourkhiss, M. Ouhssine, Inhibition of mild steel corrosion in 1M hydrochloric medium by the Methanolic extract of Ammi visnaga L. lamseeds, *Int. J. Corrosion* 2020 (2020) 9764206, <https://doi.org/10.1155/2020/9764206>.
- [108] Y. Qiang, S. Zhang, L. Guo, X. Zheng, B. Xiang, S. Chen, Experimental and theoretical studies of four allyl imidazolium-based ionic liquids as green inhibitors for copper corrosion in sulfuric acid, *Corros. Sci.* 119 (2017) 68–78, <https://doi.org/10.1016/j.corsci.2017.02.021>.
- [109] R. Ansari, M.A. Quraishi, A. Singh, Schiff's base of pyridyl substituted triazoles as new and effective corrosion inhibitors for mild steel in hydrochloric acid solution, *Corros. Sci.* 79 (2014) 5–15, <https://doi.org/10.1016/j.corsci.2013.10.009>.
- [110] A. S. Fouda, R. E. Ahmed and A. El-Hossiany, Chemical, Electrochemical and Quantum Chemical Studies for Famotidine Drug as a Safe Corrosion Inhibitor for a-Brass in HCl Solution, *Prot. Met. Phys.Chem. Surf.*, 57(2)(2021)398–411.
- [111] S. Mo, T.T. Qin, H.Q. Luo, N.B. Li, Insights into the corrosion inhibition of copper in hydrochloric acid solution by self-assembled films of 4-octylphenol, *RSC Adv.* 5 (2015) 90542–90549, <https://doi.org/10.1039/C5RA13074C>.
- [112] A.A. Al-Amiery, F.A. Binti Kassim, A. Amir, H. Kadhum, A. Bakar Mohamad, Synthesis and characterization of a novel eco-friendly corrosion inhibition for mild steel in 1M hydrochloric acid, *Sci. Rep.* 6 (2016) 19890, <https://doi.org/10.1038/srep1989>.
- [113] B. Tan, B. Xiang, S. Zhang, Y. Qiang, L. Xu, S. Chen, J. He, Papaya leaves extract as a novel eco-friendly corrosion inhibitor for Cu in H<sub>2</sub>SO<sub>4</sub> medium, *Journal of Colloid and Interface Science* 582 (2021) 918–931. <https://doi.org/10.1016/j.jcis.2020.08.093>
- [114] C. Jing, Z. Wang, Y. Gong, H. Huang, Y. Ma, H. Xie, H. Li, S. Zhang, F. Gao, Photo and thermally stable branched corrosion inhibitors containing two benzotriazole groups for copper in 3.5 wt% sodium chloride solution, *Corros. Sci.* 138 (2018) 353–371. <https://doi.org/10.1016/j.corsci.2018.04.027>
- [115] A. S. Fouda, S. M. Rashwan, M. M. K. Darwish and N. M. Arman, Corrosion Inhibition of Zn in a 0.5 M HCl Solution by Ailanthus altissima Extract, *Port. Electrochim. Acta*, 36(5)(2018) 309–323.

- [116] A.S. Fouda, S.M. Rashwan, M.M.K. Darwish, N.M. Arman, Corrosion Inhibition of Zn in a 0.5 M HCl Solution by *Ailanthus altissima* Extract, *Port. Electrochim. Acta* 36 (5) (2018) 309–323.
- [117] M. Mobin, I. Ahmada, M. Murmu, P. Banerjee, R. Aslam, Corrosion inhibiting properties of polysaccharide extracted from *Lepidium meyenii* root for mild steel in acidic medium: Experimental, density functional theory, and Monte Carlo simulation studies, *J. Phys. Chem. Solids*, 179(2023) 111411, <https://doi.org/10.1016/j.jpcs.2023.111411>
- [118] E.E. El-Katori, A.S. Fouda, R.R. Mohamed, Synergistic corrosion inhibition activity of the *chicoriumintybus* extract and iodide ions for mild steel in acidic media, *J. Chil. Chem. Soc.* 65 (1) (2020) <https://doi.org/10.4067/S0717-97072020000104672>.
- [119] A.S. Fouda, F.Sh. Mohamed, M.W. El-Sherbeni, Corrosion inhibition of aluminum–silicon alloy in hydrochloric acid solutions using Carbamidic Thioanhydride derivatives, *J. Bio. Tribo. Corros.* 2 (2016) 11, <https://doi.org/10.1007/s40735-016-0039-y>.
- [120] Y. B. Ran , M. Li , Q. Xu , Jian Peng, GO-functionalized MXene towards superior anti-corrosion coating, *Journal of Colloid and Interface Science* 642 (2023) 595–603. <https://doi.org/10.1016/j.jcis.2023.03.167>
- [121] H. Li , Y. Qiang , W. Zhao, Shengtao Zhang, 2-Mercaptobenzimidazole-inbuilt metal-organic-frameworks modified graphene oxide towards intelligent and excellent anti-corrosion coating, *Corrosion Science* 191 (2021) 109715. <https://doi.org/10.1016/j.corsci.2021.109715>
- [122] A. M. Eid, S. Shaaban and K. Shalabi, Tetrazole-based organoselenium bi-functionalized corrosion inhibitors during oilwell acidizing: experimental, computational studies, and SRB bioassay, *J. Mol. Liq.*, 298(2020) 111980, DOI: [10.1016/j.molliq.2019.111980](https://doi.org/10.1016/j.molliq.2019.111980).
- [123] Handbook of X-ray Photoelectron Spectroscopy, ed. J. F. Moulder, W. F. Stickle, P. E. Sobol and K. D. Bomben, Published by Perkin-Elmer Corporation Physical Electronics Division, 6509 Flying Cloud Drive Eden Prairie, MinnCSOLA 55344 United States of America, 1992.
- [124] R. Aslam , M. Mobin , Huda , M. Murmu , P. Banerjee, J. Aslam, L-Alanine methyl ester nitrate ionic liquid: synthesis, characterization and anti-corrosive application, *J. Mol. Liq.*, 334 (2021) 116469. <https://doi.org/10.1016/j.molliq.2021.116469>
- [125] R. Aslam , M. Mobin , Huda , M. Shoeb , M. Murmu , P. Banerjee , Proline nitrate ionic liquid as high temperature acid corrosion inhibitor for mild steel: Experimental and molecular-level insights, *J. Indus. Eng. Chem.*, 100 (2021) 333–350, <https://doi.org/10.1016/j.jiec.2021.05.005>
- [126] A.S. Fouda, H.M. Killa, A. Farouk, A.M. Salem, Calicotome Extract as a Friendly Corrosion Inhibitor of Carbon Steel in Polluted NaCl (3.5% NaCl + 16 ppm Na<sub>2</sub>S): Chemical and Electrochemical Studies, *Egypt. J. Chem.* 62 (10) (2019) 1879–1894, <https://doi.org/10.21608/ejchem.2019.7656.1649>
- [127] M.A. Bedair, M.M.B. El-Sabbah, A.S. Fouda, H.M. Elaryian, Synthesis, electrochemical and quantum chemical studies of some prepared surfactants based on azodye and Schiff base as corrosion inhibitors for steel in acid medium, *Corros. Sci.* 128 (2017) 54–72, <https://doi.org/10.1016/j.corsci.2017.09.016>.
- [128] M. Honarvar Nazari, M. Salih Shihab, Eden Adele Havens<sup>1</sup> and Xianming Shi, Mechanism of corrosion protection in chloride solution by an apple-based green inhibitor: experimental and theoretical studies, *J. Infrastr. Preserv. Resilience* 1 (2020) 7–25, <https://doi.org/10.1186/s43065-020-00007-w>.
- [129] M. H. Nazari, M. S. Shihab, E. A. Havens and X. Shi, Mechanism of corrosion protection in chloride solution by an apple-based green inhibitor: experimental and theoretical studies, *J. Infrastruct. Preserv. Resilience*, (1)2020, 7–25, DOI: [10.1186/s43065-020-00007-w](https://doi.org/10.1186/s43065-020-00007-w).
- [130] Y. El Kacimi, R. Tourir, K. Alaoui, S. Kaya, A. Salem Abousalem, M. Ouakki, M. Ebn Touhami, Anti-corrosion properties of 2-Phenyl-4(3H)-quinazolinone-substituted compounds: electrochemical, quantum chemical, Monte Carlo, and molecular dynamic simulation investigation, *J. Bio-Tribo-Corrosion* 6 (2020) 47–71, <https://doi.org/10.1007/s40735-020-00342-1>.
- [131] Y. Koumya, R. Idouhli, A. Oukhrib, M. Khadiri, A. Abouelfida, A. Benyaich, Synthesis, electrochemical, thermodynamic, and quantum chemical investigations of amino Cadalene as a corrosion inhibitor for stainless steel type 321 in sulfuric acid 1M, *Int. J. Electrochem.* 2020 (2020) 5620530–5620540, <https://doi.org/10.1155/2020/5620530>.
- [132] S. Ramesh Kumar, M. Rashvand Avei, M. Vijayan, Electrochemical and Quantum Chemical Studies on Corrosion Inhibition Performance of 2,2'-(2-Hydroxyethylimino)bis[N-(alpha,alpha-dimethylphenethyl)-N-methylacetamide] on Mild Steel Corrosion in 1M HCl Solution, *Mater. Res.* 23 (2) (2020) e20180610, <https://doi.org/10.1590/1980-5373-MR-2018-0610>.

- [133] S. RameshKumar, M. RashvandAvei and M. Vijayan, Electrochemical and Quantum Chemical Studies on Corrosion Inhibition Performance of 2,20-(2-Hydroxyethylimino)bis[N-(alphaalphadimethylphenethyl)-N-methylacetamide] on Mild Steel Corrosion in 1 M HCl Solution, *Mater. Res.*, 2020, 23(2),e20180610, [doi:10.1590/1980-5373-MR-2018-0610](https://doi.org/10.1590/1980-5373-MR-2018-0610).
- [134] B. D. Mert, M. E. Mert, G. Kardas and B. Yazici, Experimental and theoretical investigation of 3-amino-1, 2, 4-triazole-5-thiol as a corrosion inhibitor for carbon steel in HCl medium, *Corros. Sci.*, 53(12)(2011) 4265–4272, [DOI: 10.1016/j.corsci.2011.08.038](https://doi.org/10.1016/j.corsci.2011.08.038).
- [135] G. Gece, The use of quantum chemical methods in corrosion inhibitor studies, *Corros. Sci.*, 2008, 50, 2981–2992, [DOI: 10.1016/j.corsci.2008.08.043](https://doi.org/10.1016/j.corsci.2008.08.043).
- [136] K. R. Ansari, S. Ramkumar, D. Nalini and M. A. Quraishi, Studies on adsorption and corrosion inhibitive properties of quinoline derivatives on N80 steel in 15% hydrochloric acid, *Cogent Chem.*, 2016, 2, 1145032–1145045, [DOI:10.1080/23312009.2016.1145032](https://doi.org/10.1080/23312009.2016.1145032).
- [137] B. D. Mert, M. E. Mert, M. E. Kardas and G. Yazici, Experimental and theoretical investigation of 3-amino-1,2, 4-triazole-5-thiol as a corrosion inhibitor for carbon steel in HCl medium, *Corros. Sci.*, 2011, 53, 4265–4272, [DOI: 10.1016/j.corsci.2011.08.038](https://doi.org/10.1016/j.corsci.2011.08.038).
- [138] N. Vu, P. Hien, M. Mathesh, V. Thu and N. Nam, Improved Corrosion Resistance of Steel in Ethanol Fuel Blend by Titania Nanoparticles and Aganonerion polymorphum Leaf Extract., *Adv. Mater. Sci. Eng.*, 2019, 4, [DOI: 10.1021/acsomega.8b02084](https://doi.org/10.1021/acsomega.8b02084).
- [139] I. Lukovits, E. Lalman and F. Zucchi, Corrosion Inhibitors—Correlation between Electronic Structure and Efficiency, *Corrosion*, 57(2001) 3–8, [DOI: 10.5006/1.3290328](https://doi.org/10.5006/1.3290328).
- [140] W. Zhang, Y. Liu, Y. Zhang, Li-J. Wang, Y.-C. Wu and H.-J. Li, 9-Substituted acridines as effective corrosion inhibitors for mild steel: electrochemical, surface morphology, and computational studies, *New J. Chem.*, 44(2020) 6464–6474, [DOI: 10.1039/d0nj00440e](https://doi.org/10.1039/d0nj00440e).
- [141] Y. Boughoues, a M. Benamira, L. Messaadia, N. Bouider and S. Abdelaziz, Experimental and theoretical investigations of four amine derivatives as effective corrosion inhibitors for mild steel in HCl medium, *RSC Adv.*, 10(2020) 24145–24158, [DOI: 10.1039/d0ra03560b](https://doi.org/10.1039/d0ra03560b).
- [142] K. Shalabi, Y. M. Abdallah, H. M. Hassan and A. S. Fouda, Adsorption and Corrosion Inhibition of Atropa Belladonna Extract on Carbon Steel in 1 M HCl Solution, *Int. J. Electrochem. Sci.*, 9(2014) 1468–1487.
- [143] M. Mobin, R. Aslama, R. Salim, Savaş Kaya, An investigation on the synthesis, characterization and anti-corrosion properties of choline based ionic liquids as novel and environmentally friendly inhibitors for mild steel corrosion in 5% HCl, *Journal of Colloid and Interface Science* 620 (2022) 293-312
- [144] O. Dagdag, Z. Sa□, H. Erramli, O. Cherkaoui, N. Wazzan, L. Guo, C. Verma, E. Ebenso and A. El Haram, Adsorption and anticorrosive behavior of aromatic epoxy monomers on carbon steel corrosion in acidic solution: computational studies and sustained experimental studies, *RSC Adv.*, (9)(2019) 14782–14796, [DOI: 10.1039/c9ra01672d](https://doi.org/10.1039/c9ra01672d).
- [145] Y. Qiang, S. Zhang, S. Xu and W. Li, Experimental and theoretical studies on the corrosion inhibition of copper by two indazole derivatives in 3.0% NaCl solution, *J. Colloid Interface Sci.*, 2016, 472, 52–59, [DOI: 10.1016/j.jcis.2016.03.023](https://doi.org/10.1016/j.jcis.2016.03.023).
- [146] J. Aslam, M. Mobin, Huda, A. Aslam & R. Aslam, Corrosion inhibition performance of multi-phytoconstituents from Eucalyptus bark extract on mild steel corrosion in 5% HCl solution, *Int. J. Environ. Sci. Technol.* 20, 2441–2454 (2023). <https://doi.org/10.1007/s13762-022-04152-5>
- [147] Y. Qiang, S. Zhang, L. Wang, Understanding the adsorption and anticorrosive mechanism of DNA inhibitor for copper in sulfuric acid, *Appl. Surf. Sci.* 492 (2019) 228-238.
- [148] D. K. Lavanya, F. V. Priya and D. P. Vijaya, Green approach to corrosion inhibition of mild steel in hydrochloric acid by 1-[Morpholin-4-yl(thiophen-2-yl)methyl]thiourea, *J. Fail. Anal. Prev.*, 20(2020) 494–502, [DOI: 10.1007/s11668-020-00850-9](https://doi.org/10.1007/s11668-020-00850-9).
- [149] K. Aramaki, N. Hagiwara and H. Nishihara, The synergistic effect of anions and the ammonium cation on the inhibition of iron corrosion in acid solution, *Corros. Sci.*, 1987, 27, 487–497, [DOI: 10.1016/0010-938X\(87\)90092-8](https://doi.org/10.1016/0010-938X(87)90092-8).
- [150] M. Morad, J. Morvan and J. Pagetti, Proceedings of the 8<sup>th</sup> European Symposium on Corrosion Inhibitors (8SEIC), *Ann. Univ. Ferrara, NS, Sez. V*, 1995, Suppl. 10, pp. 159–167.
- [151] A. Yurt, B. Duran and H. Dal, An experimental and theoretical investigation on adsorption properties of some diphenolic Schiff bases as corrosion inhibitors at acidic solution/mild steel interface, *Arab. J. Chem.*, 2014, 7, 732–740, [DOI: 10.1016/j.arabjc.2010.12.010](https://doi.org/10.1016/j.arabjc.2010.12.010).

- 
- [152] K. A. Alamry, R. Aslam , Ajahar Khan , Mahmoud A. Hussein , Nada Y. Tashkandi , Evaluation of corrosion inhibition performance of thiazolidine-2,4-diones and its amino derivative: Gravimetric, electrochemical, spectroscopic, and surface morphological studies, *Process Saf. Environ. Prot.*, 159 (2022) 178-197, <https://doi.org/10.1016/j.psep.2021.12.061>
- [153] M. Benahmed, N. Djeddi, S. Akkal and H. Laouer, Saccocalyx satureioides as corrosion inhibitor for carbon steel in acid solution, *Int. J. Ind. Chem.*, 7(2016) 109–120, DOI: [10.1007/s40090-016-0082-z](https://doi.org/10.1007/s40090-016-0082-z).
- [154] J. Aslam , R. Aslam , S. Hamed Alrefae , M. Mobin , A.Aslam , M. Parveen , C. M. Hussain, Gravimetric, electrochemical, and morphological studies of an isoxazole derivative as corrosion inhibitor for mild steel in 1M HCl, *Arab. J. of Chem.* (2020) 7744-7758. <https://doi.org/10.1016/j.arabjc.2020.09.008>